



# H<sub>2</sub>O and HCl trace gas kinetics on crystalline HCl hydrates and amorphous HCl/H<sub>2</sub>O in the range 170 to 205 K: the HCl/H<sub>2</sub>O phase diagram revisited

R. Iannarelli and M. J. Rossi

Laboratory of Atmospheric Chemistry (LAC), Paul Scherrer Institute (PSI), PSI Villigen, 5232, Switzerland

Correspondence to: M. J. Rossi (michel.rossi@psi.ch)

Received: 7 November 2013 – Published in Atmos. Chem. Phys. Discuss.: 27 November 2013

Revised: 24 March 2014 – Accepted: 10 April 2014 – Published: 27 May 2014

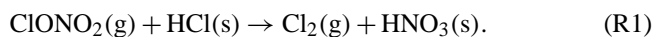
**Abstract.** In this laboratory study, H<sub>2</sub>O ice films of 1 to 2 μm thickness have been used as surrogates for ice particles at atmospherically relevant conditions in a stirred flow reactor (SFR) to measure the kinetics of evaporation and condensation of HCl and H<sub>2</sub>O on crystalline and amorphous HCl hydrates. A multidagnostic approach has been employed using Fourier transform infrared spectroscopy (FTIR) absorption in transmission to monitor the condensed phase and residual gas mass spectrometry (MS) for the gas phase. An average stoichiometric ratio of H<sub>2</sub>O : HCl = 5.8 ± 0.7 has been measured for HCl · 6H<sub>2</sub>O, and a mass balance ratio between HCl adsorbed onto ice and the quantity of HCl measured using FTIR absorption ( $N_{\text{in}} - N_{\text{esc}} - N_{\text{ads}}$ )/ $N_{\text{FTIR}} = 1.18 \pm 0.12$  has been obtained. The rate of evaporation  $R_{\text{ev}}(\text{HCl})$  for crystalline HCl hexahydrate (HCl · 6H<sub>2</sub>O) films and amorphous HCl/H<sub>2</sub>O mixtures has been found to be lower by a factor of 10 to 250 compared to  $R_{\text{ev}}(\text{H}_2\text{O})$  in the overlapping temperature range 175 to 190 K. Variations of the accommodation coefficient  $\alpha(\text{HCl})$  on pure HCl · 6H<sub>2</sub>O up to a factor of 10 at nominally identical conditions have been observed. The kinetics ( $\alpha$ ,  $R_{\text{ev}}$ ) are thermochemically consistent with the corresponding equilibrium vapour pressure. In addition, we propose an extension of the HCl/H<sub>2</sub>O phase diagram of crystalline HCl · 6H<sub>2</sub>O based on the analysis of deconvoluted FTIR spectra of samples outside its known existence area. A brief evaluation of the atmospheric importance of both condensed phases – amorphous HCl/H<sub>2</sub>O and crystalline HCl · 6H<sub>2</sub>O – is performed in favour of the amorphous phase.

## 1 Introduction

After the discovery of the ozone hole over Antarctica, the importance of heterogeneous chemistry on frozen surfaces had started to be recognized (Solomon et al., 1986) as well as the role of polar stratospheric clouds (PSCs) as substrates on whose surfaces heterogeneous reactions may take place.

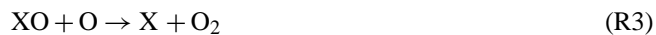
PSCs are formed in the stratosphere during polar night when the temperatures drop to as low as 183 K to allow for cloud formation even in the dry stratosphere (Peter, 1997). PSCs are classified according to their composition, consisting either of crystalline NAT (type Ia), ternary H<sub>2</sub>SO<sub>4</sub>/HNO<sub>3</sub>/H<sub>2</sub>O supercooled solution (type Ib) or pure H<sub>2</sub>O ice (type II) (Zondlo et al., 2000).

Heterogeneous reactions occurring on PSCs convert the major unreactive chlorine reservoir compounds, ClONO<sub>2</sub> and HCl, into molecular chlorine, which is rapidly photolysed into atomic chlorine. Reaction (R1) is the most important chlorine-activating reaction in the polar stratosphere because it converts two moles of unreactive chlorine compounds into two moles of atomic chlorine after photolysis in an efficient heterogeneous reaction (Seinfeld and Pandis, 2006):



Reaction (R1) belongs to one of the fastest stratospheric reactions (Friedl et al, 1986; Molina et al., 1985, 1987), orders of magnitude faster than the corresponding homogeneous gas phase process (Molina et al., 1985). The Cl<sub>2</sub> released into the gas phase from Reaction (R1) rapidly photolyses into free Cl atoms, which then establish a rapid cycle of O<sub>3</sub> destruction. Furthermore, Reaction (R1) also leads to the overall removal

of nitrogen oxides from the gas phase, trapping HNO<sub>3</sub> in the ice and thus facilitating O<sub>3</sub> destruction through a catalytic cycle as reported in Reactions (R2)–(R4):



where X is H, OH, NO, Cl or Br leading to HO<sub>x</sub>, NO<sub>x</sub>, ClO<sub>x</sub> and BrO<sub>x</sub> catalytic cycles, respectively.

The understanding of the interaction of HCl with ice is crucial in order to determine the availability of HCl at the gas–ice condensed phase interface for Reaction (R1) to effectively happen. To this purpose, the HCl–ice system has been extensively studied over the years by means of different techniques. Laminar flow tubes and Knudsen reactors are among the most widely used devices when coupled with diagnostic techniques such as ellipsometry (McNeill et al., 2006), Fourier transform infrared spectroscopy (FTIR) in transmission (Ritzhaupt and Devlin, 1991; Koehler et al., 1993; Delzeit et al., 1993) and reflection–absorption infrared spectroscopy (RAIRS) (Banham et al., 1996; Graham and Roberts, 1997). Two crystalline hydrates have been found at temperatures that may be relevant for the upper troposphere and lower stratosphere, the hexahydrate (HCl · 6H<sub>2</sub>O) and the trihydrate (HCl · 3H<sub>2</sub>O). Moreover, amorphous mixtures of variable H<sub>2</sub>O : HCl ratios, may well be relevant at stratospheric conditions.

The phase diagram of the HCl/H<sub>2</sub>O system constructed by Molina and coworkers (Molina, 1994; Wooldridge et al., 1995) indicates that the HCl trihydrate requires HCl concentrations much higher than found in the stratosphere ([HCl] = 1–3 ppb; Carslaw et al., 1997) and therefore has no atmospheric relevance. On the other hand, HCl hexahydrate may nucleate at HCl concentrations of atmospheric relevance but at temperatures lower than normally found during polar nights such that its atmospheric relevance has been questioned as well (Koehler et al., 1993; McNeill et al., 2007; Chiesa and Rossi, 2013). It thus appears that only bulk amorphous HCl/H<sub>2</sub>O mixtures have atmospheric relevance at long atmospheric residence times which are in addition more reactive than the crystalline phase HCl · 6H<sub>2</sub>O as far as Reaction (R1) is concerned (McNeill et al., 2006).

In this study we focused our attention on the HCl hexahydrate phase (HH) as well as on amorphous mixtures (amHCl) using HCl concentrations comparable to HCl hexahydrate in order to compare its behaviour under typical stratospheric conditions of [H<sub>2</sub>O] = 2–6 ppm and [HCl] = 1–3 ppb (Carslaw et al., 1997). Our results are in agreement with previous studies in showing that the irreversible conversion of HCl hexahydrate into an amorphous 6 : 1 H<sub>2</sub>O/HCl mixture was observed at temperatures higher than 190 K (Graham and Roberts, 1997; Sadtchenko et al., 2000; Chiesa and Rossi, 2013) and that the amorphous HCl/H<sub>2</sub>O phase

had a larger HCl vapour pressure, thus increased reactivity compared to crystalline HCl · 6H<sub>2</sub>O under similar experimental conditions (Chiesa and Rossi, 2013). This increased reactivity of an amorphous phase is consistent with the conclusions that a “disordered” HCl/H<sub>2</sub>O ice structure was more reactive in terms of Reaction (R1) compared to a “non-disordered” ice structure (McNeill et al., 2006).

The main focus of this study is, however, the heterogeneous kinetics of H<sub>2</sub>O and HCl interacting with crystalline HCl hexahydrate and amorphous HCl/H<sub>2</sub>O phases, which have, to our knowledge, not been studied in detail before. The majority of studies focus on the HCl interaction with ice in terms of the total uptake on pure ice films (Abbatt et al., 1992; Hanson and Ravishankara, 1992; Chu et al., 1993; Huthwelker et al., 2004) and only briefly (if not at all) mention an uptake coefficient  $\gamma$  or an accommodation coefficient  $\alpha$  of HCl on ice in the range 0.1 to 0.3. Others have studied the interaction of HCl with ice films in terms of its effects on the morphology (Sadtchenko et al., 2000) and on the disorder and roughness of the substrate surface (McNeill et al., 2007).

Hynes et al. (2001) report  $\gamma(\text{HCl}) = 0.1$  at 205 K with a substantial decrease as the temperature increases with no dependence on  $P_{\text{HCl}}$ , whereas Flückiger et al. (1998) found  $\gamma(\text{HCl})$  in the range from 0.34 to 0.22 in the temperature range 190 to 210 K on pure ice with a negative temperature dependence, which has been explained using a two-precursor model (Flückiger and Rossi, 2003). Given the nature of the experiments, namely laminar flow tubes and Knudsen reactors, neither is able to identify the nature of the substrate as they have no means of investigating the condensed phase under the relevant conditions of the uptake experiment. Using a stirred flow reactor similar to the one used in this work, Delval et al. (2003) provided a  $\gamma$  value ranging from 0.05 to 0.01 in the temperature range 200 to 235 K and are able to identify the nature of the substrate by means of FTIR in transmission.

In this work we expand on the results of Delval et al. (2003) by measuring the uptake kinetics of HCl and H<sub>2</sub>O on HCl-doped ice substrates whose phase identities are known, namely HCl hexahydrate or an amorphous HCl/H<sub>2</sub>O mixture, in the temperature range 170–205 K. Using the uptake data of several independent experimental series, we then obtain the kinetics of the two “elementary” processes, namely the mass accommodation coefficient  $\alpha(X)$  and the corresponding evaporation rate  $R_{\text{ev}}(X)$  for X = H<sub>2</sub>O and HCl. Regarding the definition of terms, we would like to refer to Ammann et al. (2013). We also discuss the effect of surface disorder on  $\alpha$ , and we propose a revision of the phase diagram of the binary HCl/H<sub>2</sub>O system based on the results obtained for the HCl hexahydrate substrates.

In order to achieve this, we have modified and adapted the reactor used by Delval et al. (2003, 2005) and Chiesa and Rossi (2013) as well as described the HCl and H<sub>2</sub>O interaction with the reactor walls using a Langmuir adsorption isotherm for both H<sub>2</sub>O and HCl, both separately and in the presence of each other, in order to resolve the difficulties in

**Table 1.** Characteristic parameters of the used stirred flow reactor (SFR).

Reactor volume (upper chamber)	2036 cm <sup>3</sup>
MS (lower) chamber	1750 cm <sup>3</sup>
Reactor internal surface (estimated)	1885 cm <sup>2</sup>
HCl calibrated volume – inlet line	62 cm <sup>3</sup>
H <sub>2</sub> O calibrated volume – inlet line	44 cm <sup>3</sup>
Si support area (one side)	A <sub>Si</sub> = 0.99 cm <sup>2</sup>
Reactor wall temperature	T <sub>w</sub> = 315 K
Gas–surface (ice sample) collision frequency	7.39 s <sup>-1</sup> (H <sub>2</sub> O)
at 315 K, one side $\omega_{\text{ice}} = \frac{4V}{c} \cdot A_{\text{Si}} = \sqrt{\frac{8RT}{\pi M}}$	5.22 s <sup>-1</sup> (HCl)
$\frac{A_{\text{Si}}}{4V} \text{ s}^{-1}$ a	
Escape rate constant <sup>b</sup>	C <sub>S</sub> = 0.0408 ± 0.0004 (small orifice)
$k_{\text{esc}}^{\text{SF}} = C_Y \cdot \sqrt{\frac{T}{M}} \text{ s}^{-1}$ , Y = S, L, S+L	C <sub>L</sub> = 0.161 ± 0.002 (large orifice)
	C <sub>S+L</sub> = 0.194 ± 0.003 (small + large orifice)
Calculated orifice area	A <sub>h</sub> (S) = 0.023 (small orifice)
$A_h = k_{\text{esc}} \cdot \frac{4V}{c} \text{ cm}^2$	(effective diameter of 1.71 cm)
	A <sub>h</sub> (L) = 0.090 (large orifice)
	(effective diameter of 3.38 cm)
	A <sub>h</sub> (S + L) = 0.108 (small + large orifice)
	(effective diameter of 3.71 cm)
Reactor wall accommodation coefficient $\alpha_w(X)$ <sup>c</sup>	(6.19 ± 0.08) × 10 <sup>-6</sup> (H <sub>2</sub> O)
	(1.69 ± 0.03) × 10 <sup>-5</sup> (HCl)

<sup>a</sup> M in kg; A<sub>Si</sub> in m<sup>2</sup>; V in m<sup>3</sup> (SI system);  $\omega$  for SFR walls ( $\omega_w$ ) is 1885/0.99 = 1904 times larger than  $\omega_{\text{ice}}$ .

<sup>b</sup> Identical value of  $k_{\text{esc}}$  under dynamic pumping conditions; M in g.

<sup>c</sup>  $k_{\text{des,w}}(X)$  may be calculated from the Langmuir equilibrium constant  $K_L$  and  $N_{\text{TOT}}(X)$  (Table 2).

the quantitative determination of HCl adsorption onto the ice substrate in transient supersaturation experiments.

## 2 Experimental apparatus

The results presented in this paper have been obtained using a modified version of a multidagnostic reactor described elsewhere (Delval et al., 2003). Figure 1 presents a scheme of the modified reactor, and Table 1 reports its characteristic parameters. Briefly, the improvements are the following: (a) introduction of a pulsed solenoid valve enabling pulsed dosing of gases – this yields the opportunity to measure the accommodation coefficient  $\alpha$  in real time; (b) use of a fast residual gas MS instrument (Prisma Plus<sup>TM</sup>) enabling the measurement of fast limiting uptake kinetics up to the gas–solid collision frequency  $\omega$ ; (c) introduction of an additional larger orifice size offering the possibility of changing the gas residence time; and (d) improvement of the temperature control resulting in ± 0.5 K deviation across the temperature range. Supplement A presents pertinent details of the hardware configuration in addition to Fig. 1 and Table 1.

## 3 Experimental methodology

The stirred-flow reactor (SFR) is characterized by a large internal surface compared to the Si substrate surface (Table 1). The SFR is a reaction vessel operated under conditions of rapid molecular stirring in relation to the gas residence time. Due to the small ratio between these areas, it is inevitable that atmospheric trace gases admitted during the experiments interact with the stainless steel chamber walls. In order to describe the interaction of H<sub>2</sub>O and HCl vapour with the low temperature ice films and the chamber walls, the following scheme has been applied:



$k_c(\text{HCl})$ ,  $R_{\text{ev}}(\text{HCl})$   
(rate of condensation on and rate of evaporation from ice)



$k_{\text{esc}}(\text{HCl})$   
(escape rate of HCl across reactor orifice)



$k_w(\text{HCl})$ ,  $R_w(\text{HCl})$   
(rate of adsorption on and rate of desorption from reactor walls)



$k_c(\text{H}_2\text{O})$ ,  $R_{\text{ev}}(\text{H}_2\text{O})$   
(rate of condensation on and rate of evaporation from ice)



$k_{\text{esc}}(\text{H}_2\text{O})$   
(rate of escape of H<sub>2</sub>O across reactor orifice)



$k_{\text{w}}(\text{H}_2\text{O}), R_{\text{w}}(\text{H}_2\text{O})$   
(rate of adsorption on and rate of desorption from reactor walls)

where  $k_{\text{c}}(\text{HCl})$  and  $k_{\text{c}}(\text{H}_2\text{O})$  are the condensation rate constants on ice in  $\text{s}^{-1}$  for HCl and H<sub>2</sub>O,  $R_{\text{ev}}(\text{HCl})$  and  $R_{\text{ev}}(\text{H}_2\text{O})$  the evaporation rates from the ice in  $\text{molec s}^{-1} \text{cm}^{-3}$ ,  $k_{\text{w}}(\text{HCl})$  and  $k_{\text{w}}(\text{H}_2\text{O})$  the adsorption rate constants onto the reactor walls,  $R_{\text{w}}(\text{HCl})$  and  $R_{\text{w}}(\text{H}_2\text{O})$  the desorption rates from the walls in  $\text{molec s}^{-1} \text{cm}^{-3}$  and  $k_{\text{esc}}(\text{HCl})$  and  $k_{\text{esc}}(\text{H}_2\text{O})$  the effusion rate constants out of the reactor in  $\text{s}^{-1}$ , respectively.

The aim of this study is to separate the rate of evaporation  $R_{\text{ev}}$  and the accommodation coefficient  $\alpha$  on ice for both gases, HCl and H<sub>2</sub>O, in order to obtain the kinetics of evaporation and condensation. Both kinetic parameters are subsequently combined to obtain the corresponding HCl and H<sub>2</sub>O equilibrium vapour pressures that may be compared to literature measurements. This approach is known as thermochemical kinetics where thermodynamic parameters are used as thermodynamic constraints for the measured kinetics.

For a gas X (HCl, H<sub>2</sub>O), the following flow balance equation holds in the presence of ice at steady state:

$$\begin{aligned} F_{\text{in}}(\text{X}) + F_{\text{des}}(\text{X}) + F_{\text{ev}}(\text{X}) \\ = F_{\text{SS}}(\text{X}) + F_{\text{ads,w}}(\text{X}) + F_{\text{ads,ice}}(\text{X}), \end{aligned} \quad (1)$$

where all terms are flow rates in  $\text{molec s}^{-1}$ . In particular,  $F_{\text{in}}$  is the chosen flow rate of molecules admitted in the reactor,  $F_{\text{des}}$  the flow rate of molecules desorbing from the reactor walls,  $F_{\text{ev}}$  the flow rate of molecules evaporating from the ice surface,  $F_{\text{SS}}$  the flow rate of molecules effusing through the leak valve into the MS chamber,  $F_{\text{ads,w}}$  the flow rate of molecules adsorbing onto the reactor walls and  $F_{\text{ads,ice}}$  the flow rate of molecules adsorbing onto the ice film.

We assume that the adsorption onto the walls can be described as a Langmuir-type adsorption, and under this assumption, Eq. (1) may be expressed as follows (see Supplement B for the mathematical derivation) for a gas X (HCl, H<sub>2</sub>O):

$$\begin{aligned} V \cdot R_{\text{in}}(\text{X}) + N_{\text{TOT}} \cdot k_{\text{des,w}}(\text{X}) \cdot \theta + V \cdot R_{\text{ev}}(\text{X}) \\ = V \cdot R_{\text{SS}}(\text{X}) + S_{\text{w}} \cdot \frac{\alpha_{\text{w}}(\text{X}) \cdot \bar{c}}{4} (1 - \theta) \cdot [\text{X}] \\ + S_{\text{ice}} \cdot \frac{\alpha_{\text{ice}}(\text{X}) \cdot \bar{c}}{4} \cdot [\text{X}], \end{aligned} \quad (2)$$

where  $V$  is the reactor volume in  $\text{cm}^3$ ,  $R_{\text{in}}$  the rate of molecules X admitted in the chamber in  $\text{molec s}^{-1} \text{cm}^{-3}$ ,

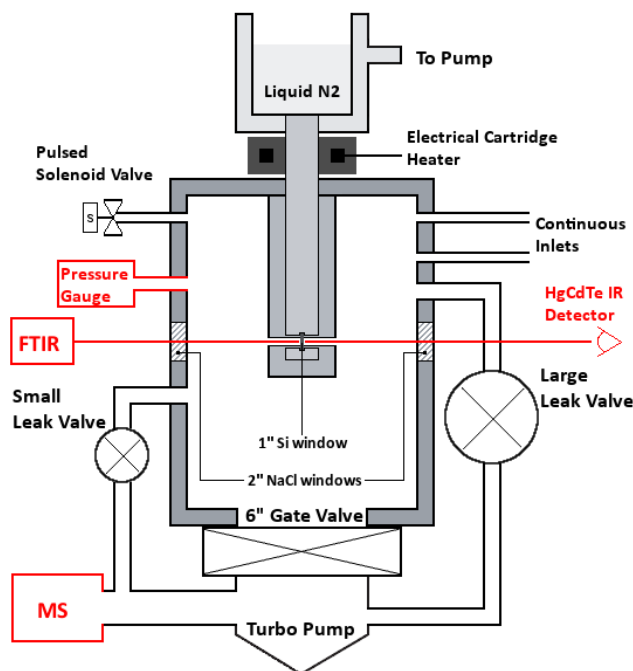


**Figure 1.** Schematic drawing of the reactor used in this work. The diagnostic tools are highlighted in red, and important parameters are listed in Table 1. The ice film is deposited on both sides of the 1" diameter Si window (black vertical symbol hanging from cryostat inside reaction vessel).

$N_{\text{TOT}}$  the total number of molecules X adsorbed onto the reactor walls,  $k_{\text{des,w}}(\text{X})$  the desorption rate constant from the reactor walls in  $\text{s}^{-1}$ ,  $\theta$  the fractional surface coverage in terms of a molecular monolayer,  $R_{\text{ev}}$  the rate of evaporation of X from the ice in  $\text{molec s}^{-1} \text{cm}^{-3}$ ,  $R_{\text{SS}}$  the rate of effusion through the leak valve in  $\text{molec s}^{-1} \text{cm}^{-3}$ ,  $S_{\text{w}}$  and  $S_{\text{ice}}$  the surfaces of the reactor walls and the ice film in  $\text{cm}^2$ ,  $\alpha_{\text{w}}$  and  $\alpha_{\text{ice}}$  the accommodation coefficients of X on the walls and on the ice film and  $\bar{c}$  the mean thermal velocity of a molecule in  $\text{cm s}^{-1}$ , respectively.

In order to measure the four unknown parameters in Eq. (2), namely  $k_{\text{des,w}}$ ,  $R_{\text{ev}}$ ,  $\alpha_{\text{w}}$  and  $\alpha_{\text{ice}}$ , a three-pronged strategy has been adopted: first, pulsed valve experiments with the cryostat at ambient temperature (no ice) have been used in order to measure  $\alpha_{\text{w}}$  for HCl and H<sub>2</sub>O. Second, the Langmuir adsorption isotherms at ambient temperature for the interaction of HCl and H<sub>2</sub>O with the reactor walls in the absence of ice have been measured and  $k_{\text{des,w}}$  has been obtained. Finally, a combination of pulsed valve and steady-state experiments has been used in order to measure  $\alpha_{\text{ice}}$  and  $R_{\text{ev}}$ , respectively, for both HCl and H<sub>2</sub>O. The details of the different steps follow below. We emphasize that the combination of a real-time (pulsed valve, PV) experiment with a steady-state flow experiment results in data of superior quality compared to the combination of two steady-state flow experiments owing to the difference of two large numbers in

the latter case. Therefore, we have used the combination of PV/steady-state flow throughout this study because the orifice sizes are not of sufficiently different size in order to afford stable numerics in the evaluation of rate data.

### 3.1 Pulsed valve experiments at room temperature

PV experiments are experiments where a transient supersaturation of gas is created in the reactor by admitting a short pulse of molecules in the range  $10^{16}$ – $10^{17}$  molecules per pulse. The admitted dose depends on the stagnant pressure of the reservoir as well as the pulse duration. In order to determine the number of molecules admitted with each pulse, the dose dependence has been calibrated using inert N<sub>2</sub> as admitted gas, yielding a typical dose of  $5.8 \times 10^{14}$  molecules per millisecond duration of the pulse per Torr of pressure in the gas reservoir. The upper limit of  $10^{17}$  molecules pulse<sup>-1</sup> leads to an upper limiting transient pressure of approximately 5 mTorr which still corresponds to molecular flow conditions.

With the cryostat at ambient temperature, PV experiments may be used to measure the uptake of HCl and H<sub>2</sub>O onto the reactor walls. In the aftermath of a calibrated pulse of known dose, the exponential decay of the mass spectrometer (MS) signal at mass  $m/z$  18 or 36 ( $k_d$ ) is given by the sum of the measured effusion ( $k_{esc}$ ) and adsorption rate constant ( $k_w$ ) on the reactor walls, namely  $k_d = k_{esc} + k_w$  (Flückiger et al., 1998).

The measured acquisition frequency of the Prisma™ control unit, expressed as the number of data points recorded per second, is approximately  $3 \text{ s}^{-1}$ , too small to measure decay rate constants in the range  $2.5$ – $0.2 \text{ s}^{-1}$  or higher. Therefore, in all PV experiments we have used a PrismaPlus™ control unit, which has an acquisition frequency of  $250 \text{ s}^{-1}$  per data point. If we take seven points in order to define a decay curve, we obtain an upper limit for the measurement of a decay rate constant of  $35 \text{ s}^{-1}$ , high enough to measure the largest rate constants we expect. These rate constants may in principle go up all the way to equal  $\omega$  in case the uptake coefficient were unity. Owing to the small sample area in the present SFR, it becomes possible to experimentally measure potentially very large uptake or accommodation coefficients which would not be possible in Knudsen or fast laminar flow reactors owing to much larger values of  $\omega$ . The dose admitted with each pulse has been calibrated using a non-reactive gas and measuring the total number of molecules admitted in the aftermath of a pulse as a function of the pulse duration and the reservoir backing pressure by time-integrating the calibrated MS signal that itself was calibrated using a steady-state flow of the same gas coupled to a measurement of the pressure decrease with time in a calibrated volume.

Figure S1 in the Supplement shows an example of pulses admitted into the reactor: the dark blue and red curves cor-

respond to pulses of H<sub>2</sub>O and HCl molecules, respectively in the absence of ice. Series of pulses at different doses have been used to determine the accommodation coefficients  $\alpha_w$ , which are related to the adsorption rate constants as follows:

$$\alpha_w = \frac{k_w}{\omega_w}, \quad (3)$$

where  $\omega_w$  is the calculated gas–surface collision frequency in  $\text{s}^{-1}$  scaled to the internal walls of the SFR and given in Table 1.

The accommodation coefficient of H<sub>2</sub>O on the walls is  $\alpha_w(\text{H}_2\text{O}) = (6.19 \pm 0.08) \times 10^{-6}$  and is roughly 4 orders of magnitude smaller than the measured  $\alpha_{ice}(\text{H}_2\text{O})$  at temperatures in the range 170 to 200 K, namely  $\alpha_{ice}(\text{H}_2\text{O}) \approx 0.1$  (see below). Since the ratio between the internal wall and the ice surface area is approximately 1000, we consider the internal walls as an active surface that can act as a source or a sink for H<sub>2</sub>O vapour, depending on its partial pressure. The contribution of the walls is even more important for HCl: the accommodation coefficient of HCl vapour on the walls is  $\alpha_w(\text{HCl}) = (1.69 \pm 0.03) \times 10^{-5}$ , only a factor of 70 smaller than the lowest value of  $\alpha_{ice}(\text{HCl}) = 1.2 \times 10^{-3}$  corresponding to the worst case scenario for HCl (Table 1).

### 3.2 Langmuir adsorption isotherms for H<sub>2</sub>O and HCl on stainless-steel reactor walls at room temperature

In this work, we assumed that the adsorption onto the walls may be described as a Langmuir adsorption. Under this assumption, the coverage of the surface walls  $\theta$  is a function of the concentration of the gas X (HCl, H<sub>2</sub>O) as follows:

$$\theta([X]) = \frac{K_L[X]}{1 + K_L[X]}, \quad (4)$$

where  $K_L$  ( $\text{cm}^3 \text{ molec}^{-1}$ ) is the Langmuir constant, which is the equilibrium constant for the adsorption process, namely  $K_L = k_c(X)/R_{ev}(X)$ , where  $k_c(X)$  is the condensation rate constant in  $\text{s}^{-1}$ . When steady-state conditions are established, the concentration of a gas X (X = H<sub>2</sub>O, HCl) in the SFR reactor is given by Eq. (5):

$$[X]_{SS} = \frac{F_{SS}(X)}{k_{esc}(X) \cdot V}. \quad (5)$$

In order to obtain the coverage  $\theta$ , we introduce a controlled flow of a gas X into the chamber at SFR conditions and wait for steady state to be established by monitoring the effusion flow using the MS. For non-interactive gases, the timescale to reach steady-state conditions is given by the residence time  $\tau_r = k_{esc}^{-1}$ . Any decrease beyond  $\tau_r$  has been attributed to the rate of adsorption of gas molecules onto the walls of the reactor, according to  $\tau_r = (k_{esc} + k_w)^{-1}$ .

Figure S2 in the Supplement shows the results of an experiment performed using HCl vapour: the grey curve represents

$n$ -steps of increasing flows of HCl effusing from the reactor as measured by the calibrated MS, corresponding to increasing HCl flows introduced into the reactor chamber. The red shaded area represents the difference between the hypothetical effusion flow  $F_{\text{esc,hypo}}$ , corresponding to a non-interactive case with no adsorption of H<sub>2</sub>O or HCl onto the walls, and the measured flow  $F_{\text{esc,meas}}$  for each  $j$ -th time interval. As mentioned above, we attribute this difference to the rate of adsorption of gas molecules onto the reactor walls. Under this assumption, for each time interval  $j$  the red shaded area in Fig. S2 in the Supplement is the total number of molecules adsorbed onto the reactor walls, which may be calculated according to Eq. (6):

$$N_{\text{ads,w}}^j(\text{X}) = \int (F_{\text{esc,hypo}}(t) - F_{\text{esc,meas}}(t)) \cdot dt, \quad (6)$$

with  $F_{\text{esc,hypo}}$  and  $F_{\text{esc,meas}}$  in  $\text{molec s}^{-1}$  and  $N_{\text{ads,w}}^j(\text{X})$ , the cumulative number of molecules X adsorbed at each  $j$ -th time interval, respectively. The total cumulative number of molecules of gas X adsorbed onto the walls  $N_{\text{ads,w}}^{\text{X}}$  is the sum of all  $N_{\text{ads,w}}^j(\text{X})$  and a function of the steady-state concentration of the gas X (HCl, H<sub>2</sub>O) and may be expressed in terms of a Langmuir constant as follows:

$$N_{\text{ads,w}}^{\text{X}}([\text{X}]) = \frac{N_{\text{TOT}}^{\text{X}} \cdot K_{\text{L}}[\text{X}]}{1 + K_{\text{L}}[\text{X}]}, \quad (7)$$

where  $N_{\text{TOT}}^{\text{X}}$  is the total maximum number of molecules X that can be adsorbed on the total internal surface of the SFR vessel. We calculated the coverage as a function of concentration as expressed in Eq. (4) as the ratio between  $N_{\text{ads,w}}^{\text{X}}$  and  $N_{\text{TOT}}^{\text{X}}$ :

$$\theta([\text{X}]) = \frac{N_{\text{ads,w}}^{\text{X}}}{N_{\text{TOT}}^{\text{X}}}. \quad (8)$$

The experiments were performed under two different conditions:

- *Pure gas system*: only one selected gas was introduced into the reactor (HCl or H<sub>2</sub>O).
- *Binary system*: the main gas has been introduced into the reactor together with a constant flow of the other gas in order to simulate the planned experiments at low temperatures.

Figure 2 shows the results for the construction of a Langmuir adsorption isotherm in terms of the wall coverage  $\theta$  obtained from Eq. (8) for HCl and H<sub>2</sub>O interacting with the stainless-steel walls at 315 K as a function of gas concentration according to Eq. (5).

The red circles represent experiments with a pure H<sub>2</sub>O flow admitted into the reactor, and the green circles represent experiments where an additional constant flow  $F_{\text{IN}} = 8 \times 10^{14} \text{ molec s}^{-1}$  of HCl was introduced into the reactor together with the variable H<sub>2</sub>O flow.

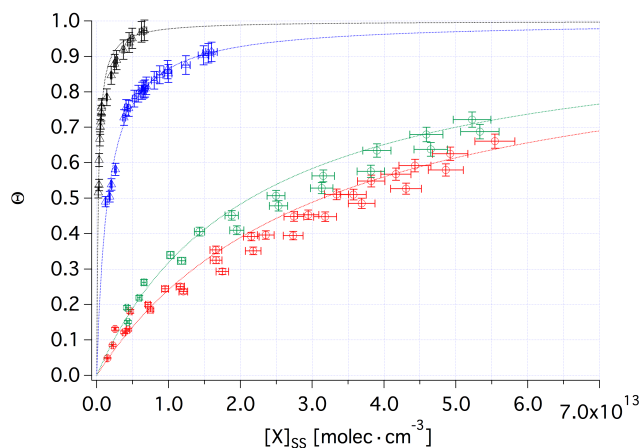


**Figure 2.** Wall coverage as a function of HCl and H<sub>2</sub>O concentration interacting with the reactor walls according to Langmuir using data of the type displayed in Fig. S2 in the Supplement. The red symbols represent the interaction of pure H<sub>2</sub>O and the green symbols the interaction of H<sub>2</sub>O in the presence of an additional HCl flow  $F_{\text{in}}(\text{HCl}) = 8 \times 10^{14} \text{ molec s}^{-1}$  admitted into the reactor. Similarly, the black symbols represent the interaction of pure HCl, the blue symbols the interaction of HCl in the presence of an additional H<sub>2</sub>O flow  $F_{\text{in}}(\text{H}_2\text{O}) = (3-6) \times 10^{15} \text{ molec s}^{-1}$  admitted into the reactor. The parameters of the fitting curves may be found in Table 2.

The black triangles represent the interaction of pure HCl, the blue triangles the interaction of HCl in the presence of an additional H<sub>2</sub>O flow admitted into the reactor. For HCl we adopted a similar approach but the results are different: in the presence of additional H<sub>2</sub>O flow, the HCl coverage is lower, in contrast to the previous case. In the following discussion we will attempt an interpretation of this difference.

$N_{\text{TOT}}$  represents the total maximum number of molecules that can be adsorbed onto the stainless-steel surface. For H<sub>2</sub>O, in the presence of HCl, it corresponds to  $N_{\text{MAX}}(\text{HCl}) = 4.45 \times 10^{14} \text{ molec cm}^{-2}$ , approximately 45 % of a formal monolayer coverage of H<sub>2</sub>O on ice (1 ML(H<sub>2</sub>O) =  $1 \times 10^{15} \text{ molec cm}^{-2}$ ), whereas for pure HCl it corresponds to  $N_{\text{MAX}}(\text{H}_2\text{O}) = 2.68 \times 10^{14} \text{ molec cm}^{-2}$ .

The number of molecules in a formal monolayer (ML) of HCl may be estimated from bulk densities using the expression  $\text{ML} = (\rho N_{\text{A}}/\text{M})^{2/3}$ , where  $\rho$ ,  $N_{\text{A}}$  and  $\text{M}$  are the bulk density, Avogadro's number and molar mass, respectively. The density  $\rho = 1.490 \text{ kg l}^{-1}$  for pure liquid HCl at  $T = -85^\circ\text{C}$  (CRC Handbook) yields a value for one ML of  $8.53 \times 10^{14} \text{ molec cm}^{-2}$ . The *Matheson Gas Data Book* provides a density of  $\rho = 0.879 \text{ kg l}^{-1}$  for liquid HCl at  $T = 10^\circ\text{C}$  and  $P = 32 \text{ atm}$ , from which a value for one ML of  $6.0 \times 10^{14} \text{ molec cm}^{-2}$  may be calculated. This last value has been used in the present work given the temperature of the reactor internal surfaces ( $T_{\text{w}} = 42^\circ\text{C}$ ) comparable to the entry given in the *Matheson Gas Data Book*. The maximum HCl coverage in the present system ( $N_{\text{MAX}} = 2.68 \times 10^{14} \text{ molec cm}^{-2}$ ) obtained from the Langmuir isotherm at saturation corresponds

therefore to approximately 45 % of a formal monolayer coverage of HCl on stainless steel. We also report that, on ice, a formal monolayer of HCl has been measured by Henson et al. (2004) as  $2.3 \times 10^{14}$  molec cm<sup>-2</sup> using BET analysis, which compares well with our measurement of  $N_{MAX}$  and points to a coverage of approximately 1 formal monolayer of HCl on the system internal surfaces on the basis of  $2.3 \times 10^{14}$  molec cm<sup>-2</sup> of HCl for a monolayer coverage on ice. However, the consensus value for HCl coverage on an ice film is closer to  $2.7 \times 10^{14}$  molec cm<sup>-2</sup> (Chiesa and Rossi, 2013).

For a gas X, the Langmuir equilibrium constant is a function of the accommodation coefficient  $\alpha_w(X)$  and the desorption rate constant  $k_{des,w}(X)$  (s<sup>-1</sup>) according to Eq. (9) (see Supplement B, Eq. S11):

$$K_L = \frac{S_W \cdot \alpha_w(X) \cdot \bar{c}/4}{N_{TOT}^X \cdot k_{des,w}(X)}, \quad (9)$$

where  $S_W$  is the internal surface in cm<sup>2</sup> and  $N_{TOT}$  the total number of adsorption sites on the surface for molecule X. The fitting parameters of the Langmuir isotherms provide  $K_L$  and  $N_{TOT}$  for the present experimental system, whereas  $\alpha_w(X)$  has been measured directly from the real-time PV observation as reported in Sect. 3.1 thus allowing the calculation of  $k_{des,w}(X)$ .

### 3.3 Pulsed valve and steady-state experiments at low temperatures

As mentioned above, a combination of PV and steady-state experiments has been used to measure  $\alpha_{ice}$  and  $R_{ev}$ , respectively, for both HCl and H<sub>2</sub>O interacting with the thin ice film. After the growth of the selected substrate according to the protocols reported above, the thin film is set to a chosen temperature. When steady-state conditions are established, a series of three gas (HCl, H<sub>2</sub>O) pulses at intervals of approximately 60 s is admitted into the reactor. Similarly to PV at room temperature, the exponential decay of the MS signal at  $m/z$  18 or 36 ( $k_d$ ) is given by the sum of the measured  $k_{esc}$ , the adsorption rate constant on the walls ( $k_w$ ) and the adsorption rate constant ( $k_{ice}$ ) onto the ice, namely  $k_d = k_{esc} + k_w + k_{ice}$ , in the aftermath of a pulse. We then calculate the accommodation coefficient  $\alpha_{ice}(X)$  of a gas X (X = HCl, H<sub>2</sub>O) onto the ice substrates according to Eq. (10) with  $\omega_{ice}$  given in Table 1:

$$\alpha_{ice} = \frac{k_{ice}}{\omega_{ice}}. \quad (10)$$

The steady-state MS signal established before the pulse series represents the flow rate of molecules effusing through the leak valve  $F_{SS}(X)$  in Eq. (1) and it may be used to calculate  $R_{ev}(X)$  from Eq. (2). Figure S3 in the Supplement shows an example of the combined PV and steady-state experiments for H<sub>2</sub>O pulses as a function of time on an HCl hexahydrate

(HH) substrate taking note of the large disparity of the MS signal for HCl and H<sub>2</sub>O. H<sub>2</sub>O flow rate with a series of pulses at temperatures of 176 and 181.5 K is shown in blue on the right axis of Fig. S3 in the Supplement. The red curve on the left axis represents the corresponding HCl flow rate at the same temperatures. At 176 K, the correspondent flow rates of H<sub>2</sub>O and HCl are measured. Subsequently, for technical reasons, only the H<sub>2</sub>O signal at  $m/z$  18 is recorded, and a series of three H<sub>2</sub>O pulses is admitted into the reactor. From the pulse decay rate  $k_d$ ,  $\alpha_{ice}(H_2O)$  may be calculated according to Eq. (10). As the temperature is increased to 181.5 K, both masses  $m/z$  18 and 36 are again recorded. When steady state is established for the new target temperature, a new series of H<sub>2</sub>O pulses is admitted. The steady-state flow before the pulse series represents  $F_{SS}(H_2O)$  in Eq. (1), and it may be used to calculate  $R_{ev}(H_2O)$  from Eq. (2). This protocol has been applied using HH and amHCl as substrates as well as alternating H<sub>2</sub>O and HCl as probing gases using a series of pulses at temperatures in the range 167 to 203 K. The orange curve in Fig. S1 in the Supplement shows an example of HCl pulses over ice, compared to a pulse (red curve) in the absence of ice.

With the separation of  $R_{ev}$  and  $\alpha_{ice}$  for both HCl and H<sub>2</sub>O, we may calculate the equilibrium vapour pressure  $P_{eq}(X)$  for each gas, corrected according to Eq. (S2) in the Supplement, as follows:

$$P_{eq}(X) = \frac{R_{ev}(X)}{k_c(X)} \cdot \frac{RT}{N_A}, \quad (11)$$

where  $R$  is the molar gas constant in cm<sup>3</sup> Torr K<sup>-1</sup> mol<sup>-1</sup>,  $T$  the temperature of the thin film in K and  $N_A$  the Avogadro constant in molec mol<sup>-1</sup>. In our current setup only one gas at a time can be used for PV experiments. When the ice film is exposed to a transient supersaturation of H<sub>2</sub>O and  $\alpha_{ice}(H_2O)$  and  $F_{SS}(H_2O)$  are measured, we may calculate  $P_{eq}(H_2O)$ , whereas only  $F_{SS}(HCl)$  can be measured, as shown in Fig. S3 in the Supplement.

The flow  $F_{SS}(HCl)$  may still be used to calculate  $P_{eq}(HCl)$  in H<sub>2</sub>O-PV experiments when coupled with  $\alpha_{ice}(HCl)$  measured in HCl-PV experiments according to Eqs. (2) and (11).

Similarly, when the ice film is exposed to an HCl pulse, both  $\alpha_{ice}(HCl)$  and  $F_{SS}(HCl)$  are measured in order to calculate  $P_{eq}(HCl)$  and only  $F_{SS}(H_2O)$  is obtained.  $F_{SS}(H_2O)$  is then coupled with  $\alpha_{ice}(H_2O)$  from H<sub>2</sub>O-PV experiments in order to calculate  $P_{eq}(H_2O)$  in HCl-PV experiments.

## 4 Results

In the following section the results obtained applying the method described above will be presented. As mentioned before, once the selected substrate, amHCl or HH, has been grown according to the corresponding protocol and characterized using its FTIR absorption spectrum (see below), the film is set to a chosen temperature. When

steady-state conditions are established, the corresponding flows  $F_{SS}(\text{H}_2\text{O})$  and  $F_{SS}(\text{HCl})$  are recorded. Subsequently, the series of gas X (HCl, H<sub>2</sub>O) pulses are admitted into the reactor, from which  $\alpha_{ice}(X)$  may be calculated according to Eq. (10). The film is then set to a higher temperature,  $F_{SS}(\text{H}_2\text{O})$  and  $F_{SS}(\text{HCl})$  are recorded and the series of pulses repeated on the same ice sample. The cumulative dose on the ice sample has been measured as the difference between the admitted dose and the number of molecules effused from the reactor in the aftermath of each pulse. This experimental protocol has been repeated for each measured point in the temperature interval of interest and repeated for both series of gas, HCl and H<sub>2</sub>O, pulses.

#### 4.1 Amorphous HCl/H<sub>2</sub>O mixture thin films

The results for amHCl are reported in Fig. 3. Figure 3a shows the measured  $\alpha_{ice}(X)$ ,  $X = (\text{H}_2\text{O}, \text{HCl})$ , as a function of temperature.  $\alpha_{ice}(\text{H}_2\text{O})$  on pure ice (inverse blue triangles) varies from 0.12 at 175 K to 0.054 at 203 K.  $\alpha_{ice}(\text{H}_2\text{O})$  on amHCl (red circles) decreases as a function of temperature, being equal to  $\alpha_{ice}(\text{H}_2\text{O})$  on pure ice within experimental error in the range 175–185 K and lower by approximately 20 % at temperatures higher than 185 K. Coloured triangles represent results for  $\alpha_{ice}(\text{HCl})$  on amHCl, where the colour scale gives the accumulated dose of HCl on the HCl-doped ice film after each pulse.  $\alpha_{ice}(\text{HCl})$  is equal within experimental error to  $\alpha_{ice}(\text{H}_2\text{O})$  on pure ice up to 180 K and lower by a factor of approximately 2 above 180 K. Consistent with the experimental protocol, the ice samples are increasingly enriched in HCl as the temperature increases. Fresh ice samples have been exposed to HCl pulses at temperatures of 194 and 200 K, and  $\alpha_{ice}(\text{HCl})$  is higher by a factor of 1.5 and 1.25 compared to aged samples, respectively. This result compares favourably with the observation of Flückiger et al. (1998), who have noticed a dose dependence of the kinetics of HCl adsorption on pure ice exposed to transient supersaturation.

Figure 3b shows results for  $R_{ev}$  in  $\text{molec s}^{-1} \text{cm}^{-3}$  as a function of temperature. Inverse blue triangles represent  $R_{ev}$  of pure ice, red circles H<sub>2</sub>O and black triangles HCl results, respectively.  $R_{ev}(\text{HCl})$  is significantly different, lower by a factor of 10 in the temperature range 175–185 K and lower by up to a factor of 100 at temperatures higher than 185 K compared to  $R_{ev}(\text{H}_2\text{O})$ , which is equal to  $R_{ev}(\text{H}_2\text{O})$  of pure ice across the temperature range 175–205 K. This result further confirms the finding of Delval et al. (2003) that the evaporation of H<sub>2</sub>O, despite the presence of adsorbed HCl onto the ice substrate, takes place at a rate characteristic of pure ice in a H<sub>2</sub>O-enriched substrate, which is at a low HCl content of the condensed phase. The full green line shows the rate of evaporation of pure water for the system in use calculated from literature results of equilibrium vapour pressure (Marti and Mauersberger, 1993) using  $\alpha = 1$ , whereas the dashed green line represents extrapolated values of  $R_{ev}(\text{H}_2\text{O})$  for

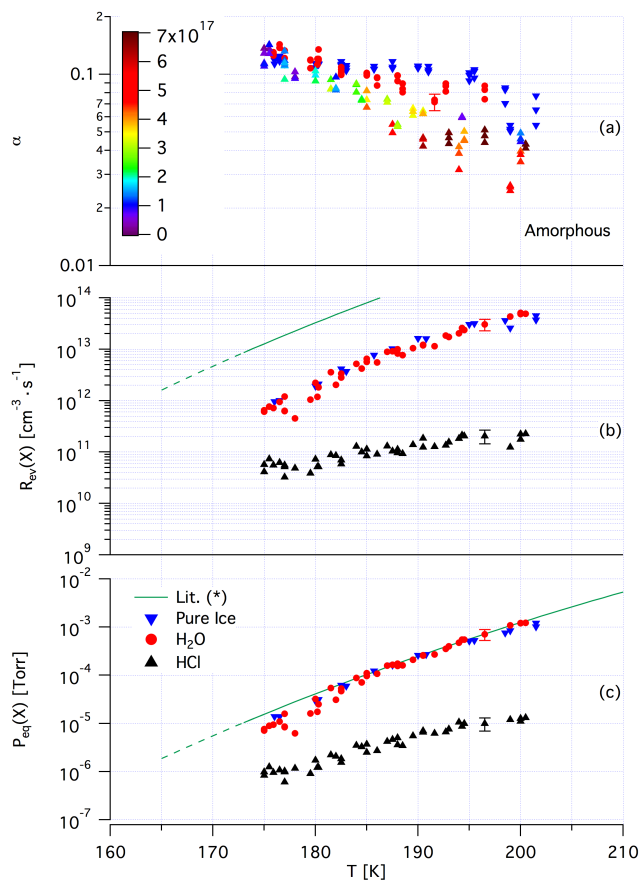


**Figure 3.** Synopsis of kinetic results for amHCl using H<sub>2</sub>O, HCl as a probe gas. The symbols used are explained in the text. The calculated relative error for  $\alpha$  is 10 %. The relative errors calculated for  $R_{ev}(\text{HCl})$  and  $P_{eq}(\text{HCl})$  are 30 %, whereas for  $R_{ev}(\text{H}_2\text{O})$  and  $P_{eq}(\text{H}_2\text{O})$  they are 25 %. Examples of the amplitude of the errors are reported for selected points. The green line shows results from Marti and Mauersberger (1993). The colour scale shows the cumulative adsorbed dose after HCl pulsed gas admission.

temperatures lower than 173 K using the expression provided by Marti and Mauersberger (1993).

Figure 3c shows the results for  $P_{eq}$  in Torr calculated according to Eq. (11) for both H<sub>2</sub>O and HCl. The same symbols as in Fig. 3b are used.  $P_{eq}(\text{HCl})$  of amHCl is lower by a factor of 100 at temperatures higher than 185 K compared to  $P_{eq}(\text{H}_2\text{O})$  of amHCl, which is equal within experimental uncertainty to  $P_{eq}(\text{H}_2\text{O})$  of pure ice. At temperatures lower than 185 K,  $P_{eq}(\text{HCl})$  of amHCl is still lower than  $P_{eq}(\text{H}_2\text{O})$  of amHCl but only by a factor of 10, less so than at higher temperatures. The solid and dashed green lines represent the vapour pressure of water as in Fig. 3b.

The values obtained for the equilibrium vapour pressure have been compared with the HCl/H<sub>2</sub>O phase diagram constructed by Molina and coworkers (Abbatt, 1992; Molina, 1994; Wooldridge, 1995). Figure 4 shows the results for amHCl films, which all lie within the existence area of HH.

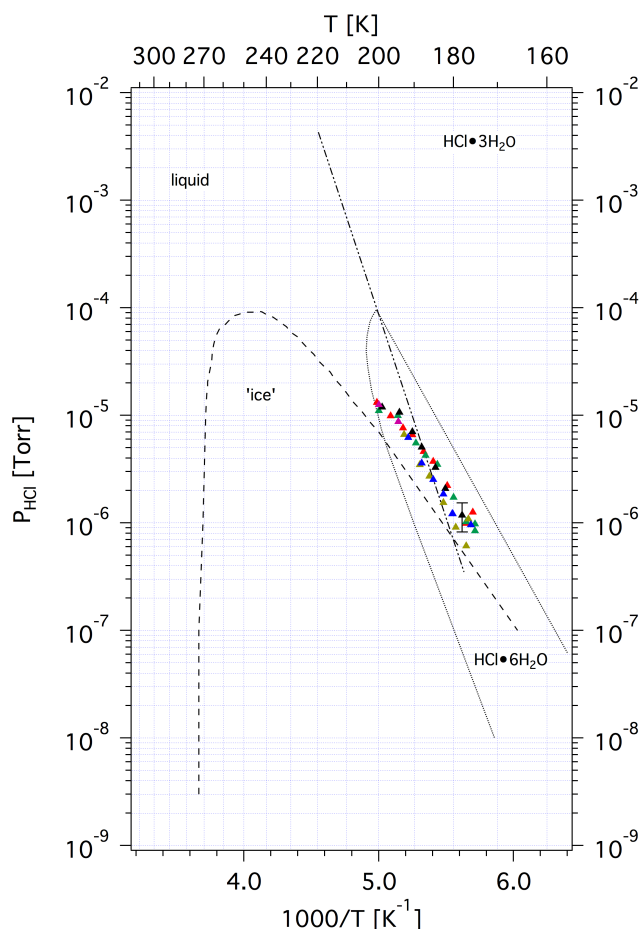


**Figure 4.** Binary phase diagram of the HCl/H<sub>2</sub>O system reconstructed from Molina and coworkers (Abbatt, 1992; Molina, 1994; Wooldridge, 1995). The full triangles represent calculated values of  $P_{\text{eq}}(\text{HCl})$  for amHCl using the kinetic data of the present work. Different colours represent different experiment series.

This is expected since the cumulative dose admitted into the reactor chamber is the same used during the HH growth protocol, namely  $5 \times 10^{17}$  molecules of HCl compared to approximately  $4 \times 10^{18}$  molecules of H<sub>2</sub>O, corresponding to an average mole fraction  $\chi_{\text{HCl}} = 0.111$ .

#### 4.2 Crystalline hexahydrate films

The results for HH are reported in Fig. 5. Figure 5a shows the measured  $\alpha_{\text{ice}}(X)$  as a function of temperature. Inverse blue triangles represent  $\alpha_{\text{ice}}(\text{H}_2\text{O})$  on pure ice, as shown in Fig. 3.  $\alpha_{\text{ice}}(\text{H}_2\text{O})$  on HH (red circles) decreases as a function of temperature and is lower by a factor of approximately 1.5 than  $\alpha_{\text{ice}}(\text{H}_2\text{O})$  on pure ice at temperatures higher than 185 K. Coloured triangles represent results for  $\alpha_{\text{ice}}(\text{HCl})$  on HH, with the colour scale showing the cumulative dose of HCl on the HCl-doped ice film.  $\alpha_{\text{ice}}(\text{HCl})$  shows larger scatter compared to amHCl with a variation up to a factor of 10 for results at the same temperature across the full temper-

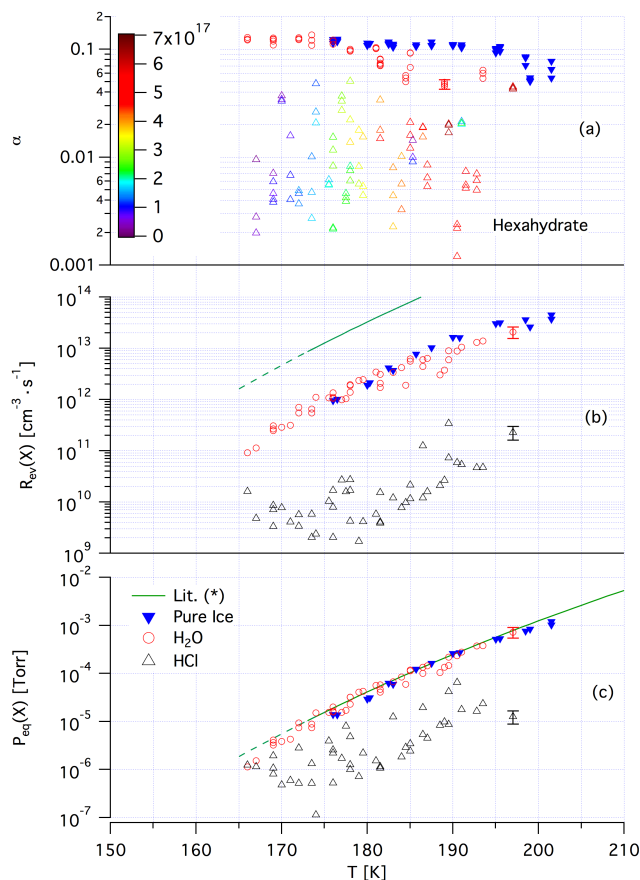


**Figure 5.** Synopsis of kinetic results for HH using H<sub>2</sub>O, HCl as a probe gas. The symbols used are explained in the text. The calculated relative error for  $\alpha$  is 10%. The relative errors calculated for  $R_{\text{ev}}(\text{HCl})$  and  $P_{\text{eq}}(\text{HCl})$  are 30%, whereas for  $R_{\text{ev}}(\text{H}_2\text{O})$  and  $P_{\text{eq}}(\text{H}_2\text{O})$  they are 25%. Examples of the amplitude of the errors are reported for selected points. The green line shows results from Marti and Mauersberger (1993). The colour scale shows the cumulative adsorbed dose after HCl pulsed gas admission.

ature range. Furthermore, each series of three pulses spaced by typically 60 to 90 s always showed a decrease in  $\alpha_{\text{ice}}(\text{HCl})$  between the first and the last pulse. Similar results have been shown previously in the literature (McNeill et al., 2007) where the scatter has been explained in terms of the morphology or the smoothness of the ice surface. We will discuss these results further in the discussion section.

Figure 5b shows results for the  $R_{\text{ev}}$  in  $\text{molec s}^{-1} \text{cm}^{-3}$  as a function of temperature.  $R_{\text{ev}}(\text{HCl})$  on HH, represented by black triangles, is lower by a factor of 100 across the temperature range 165–193 K compared to  $R_{\text{ev}}(\text{H}_2\text{O})$  on HH, which, being equal to  $R_{\text{ev}}(\text{H}_2\text{O})$  on pure ice within experimental error, indicates that the presence of crystalline HH on the ice substrate does not substantially affect the evaporation of H<sub>2</sub>O, which is that of pure ice, in a manner similar to amHCl as described before.

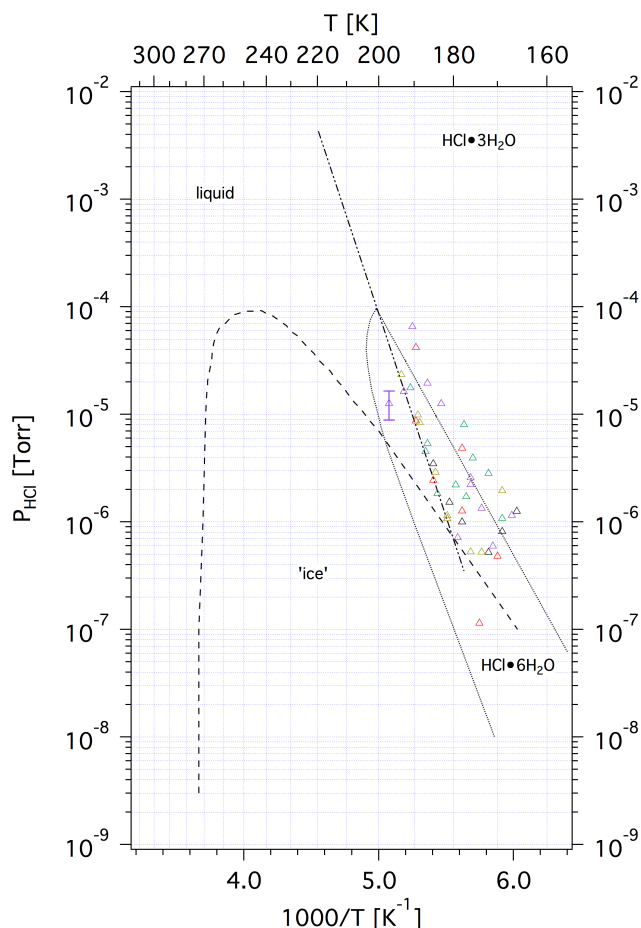


**Figure 6.** Binary phase diagram of the HCl/H<sub>2</sub>O system. The empty triangles represent calculated values of  $P_{\text{eq}}(\text{HCl})$  for HH using the kinetic data for adsorption and desorption of the present work. Different colours represent different experiment series.

Figure 5c shows the results for  $P_{\text{eq}}$  in Torr calculated according to Eq. (11) for both H<sub>2</sub>O and HCl.  $P_{\text{eq}}(\text{H}_2\text{O})$  of HH is equal to  $P_{\text{eq}}(\text{H}_2\text{O})$  of pure ice within experimental error, whereas  $P_{\text{eq}}(\text{HCl})$  of HH is lower by a factor of 4 to 15 compared to  $P_{\text{eq}}(\text{H}_2\text{O})$  of HH. The scatter of  $P_{\text{eq}}(\text{HCl})$ , being of the same magnitude as the scatter of  $\alpha_{\text{ice}}(\text{HCl})$ , may likewise be explained by a variation in the substrate composition as well as by an increase in its roughness or inhomogeneous nature due to the exposure to HCl pulses.

Figure 6 shows the phase diagram of the results obtained for HH films: most of the results lie in the HH existence region, as expected, but there is a significant number of points lying outside the HH existence area. In order to determine whether or not this result pertains to the hexahydrate phase, we took advantage of the multidagnostic capabilities of the apparatus and focused our attention to the condensed phase using the corresponding FTIR spectrum for each of the experiments in question.

### 4.3 FTIR spectra of hexahydrate

The FTIR spectrum of hexahydrate is known from the literature (Ritzhaupt and Devlin, 1991; Koehler et al., 1993; Toon et al., 1994; Graham and Roberts, 1997). For each point in Fig. 6, a corresponding spectrum of the thin film has been collected. All spectra corresponding to experiments lying in the HH existence region are a mixture of pure ice and HH film as they have the spectroscopic signature of hexahydrate phase, namely the two additional peaks in the OH stretching region at 3426 and 3366  $\text{cm}^{-1}$  and the sharp peak at 1635  $\text{cm}^{-1}$ , corresponding to the bending vibration of the proton ordered waters of hydration. Likewise, the spectra corresponding to experiments lying outside the known published HH existence region appear to be a combination of pure ice and pure HH. In order to clearly indicate the presence of HH as well as the HH to ice mixing ratio for these experiments, we deconvoluted all experimental spectra. We assume that the measured composite spectrum is a superposition of the spectra of pure ice and pure HH following Graham and Roberts (1997), and we proceeded as follows in order to deconvolute the absorption spectrum: the sharp IR peak at 1635  $\text{cm}^{-1}$  is an unambiguous marker of HH. Therefore, the optical density at this peak can be used as a marker of the amount of HH present in the ice film. We scaled the optical density at 1635  $\text{cm}^{-1}$  of an independently recorded spectrum of pure HH to that of the spectrum of interest. The scaled spectrum is that of the pure HH component, and we obtain the pure ice component from the measured composite spectrum after subtraction.

Figure S4 in the Supplement shows an example of the deconvolution: the green spectrum is the recorded spectrum, which is the superposition of pure HH and pure H<sub>2</sub>O ice; the red spectrum is the measured spectrum of pure HH scaled to the measured amplitude of the IR absorption peak at 1635  $\text{cm}^{-1}$ . The blue spectrum corresponds to the difference of the green and the red spectrum. It is obvious that the measured spectrum is that of a film where pure ice and pure HH coexist. The procedure does not take into account possible small shifts of up to  $\pm 2 \text{ cm}^{-1}$  of the pure component spectrum in the presence of the other component, commensurate with the absolute wavelength accuracy of the FTIR spectrometer in the current configuration ( $\pm 1 \text{ cm}^{-1}$ ).

Figure 7 shows the HCl/H<sub>2</sub>O phase diagram and the FTIR spectra of a few experiments outside the known HH existence area, labelled accordingly. Each spectrum panel shows the measured FTIR spectrum in the same colour as the vapour pressure plotted in the bottom left panel as well as its deconvolution into a pure ice component (blue spectrum) and a pure HH component (red spectrum). This procedure has been applied to all experiments outside the known HH existence area. For all cases the same conclusion has been reached, namely that all measured  $P_{\text{eq}}(\text{HCl})$  results in Fig. 6 indeed pertain to binary HH–ice films of various composition.

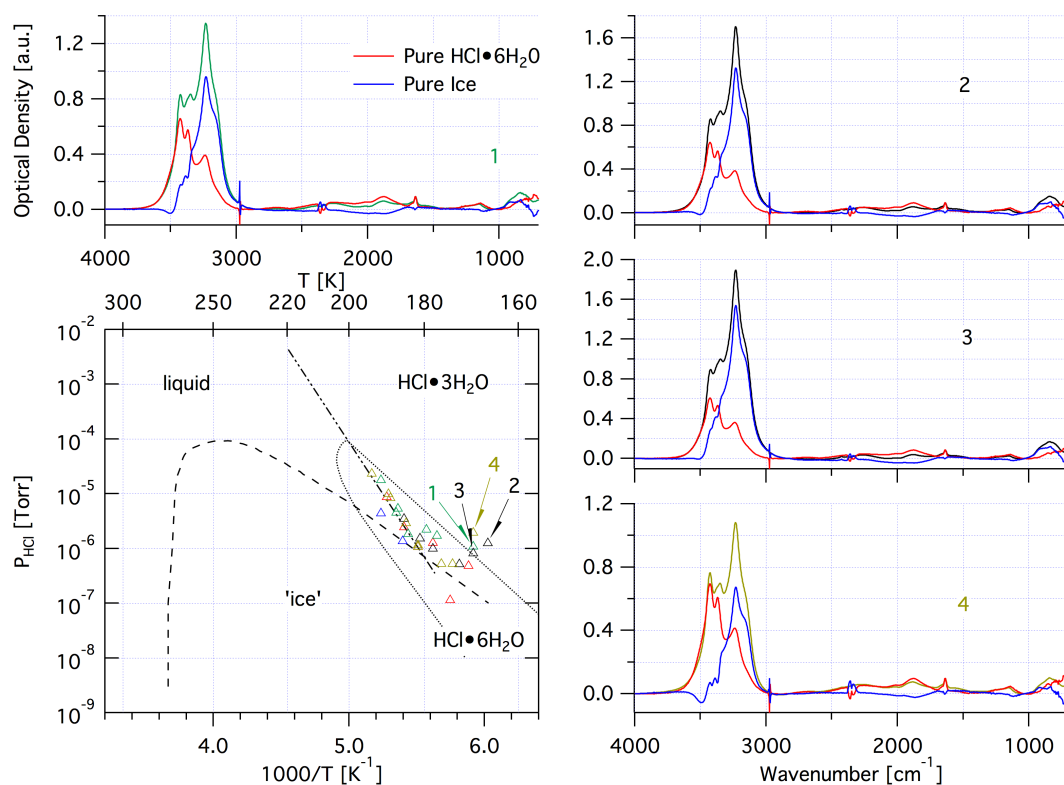


**Figure 7.** Selected measured FTIR spectra with their deconvolution into pure ice (blue) and pure HH (red) component. The measured FTIR absorption spectra are coloured according to where they fit into the binary HCl/H<sub>2</sub>O phase diagram.

**Table 2.** Fit parameters for H<sub>2</sub>O and HCl interaction with internal stainless steel surfaces (SS304) of the reactor.

	$K_L^*$ [cm <sup>3</sup> molec <sup>-1</sup> ]	$N_{TOT}$ [molec]	$N_{MAX}$ [molec cm <sup>-2</sup> ]
H <sub>2</sub> O adsorption	$(3.18 \pm 0.38) \times 10^{-14}$	$(7.03 \pm 0.42) \times 10^{17}$	$(3.73 \pm 0.22) \times 10^{14}$
H <sub>2</sub> O adsorption with HCl flow ( $F_{in} = 8 \times 10^{14}$ molec s <sup>-1</sup> )	$(4.67 \pm 0.39) \times 10^{-14}$	$(8.38 \pm 0.29) \times 10^{17}$	$(4.45 \pm 0.15) \times 10^{14}$
HCl adsorption	$(4.37 \pm 0.21) \times 10^{-12}$	$(5.06 \pm 0.06) \times 10^{17}$	$(2.68 \pm 0.03) \times 10^{14}$
HCl adsorption with H <sub>2</sub> O flow ( $F_{in} = 6 \times 10^{15}$ molec s <sup>-1</sup> )	$(6.31 \pm 0.49) \times 10^{-13}$	$(4.85 \pm 0.07) \times 10^{17}$	$(2.57 \pm 0.04) \times 10^{14}$
HCl adsorption with H <sub>2</sub> O flow ( $F_{in} = 3 \times 10^{15}$ molec s <sup>-1</sup> )	$(6.46 \pm 0.63) \times 10^{-13}$	$(3.79 \pm 0.09) \times 10^{17}$	$(2.01 \pm 0.04) \times 10^{14}$

\*  $K_L$  is the Langmuir adsorption equilibrium constant.

## 5 Discussion

### 5.1 Langmuir adsorption isotherms

In order to describe the adsorption of HCl and H<sub>2</sub>O onto the reactor internal surface, we used Langmuir adsorption isotherms to fit the measurement of HCl and H<sub>2</sub>O surface coverage. As shown in Fig. 2, the presence of an HCl flow during H<sub>2</sub>O steady-state experiments (green circles) presumably enhances the capability of H<sub>2</sub>O to adsorb onto the walls, whereas the presence of an additional H<sub>2</sub>O flow during HCl

exposure reduces the HCl coverage. The *increasing* trend of H<sub>2</sub>O adsorption in going from the pure case to H<sub>2</sub>O in the presence of HCl (going from red to green in Fig. 2) means that H<sub>2</sub>O will unselectively adsorb on both surface sites as well as on already adsorbed HCl. H<sub>2</sub>O is able to adsorb both on already adsorbed HCl as well as on free surface sites. In contrast, the *decreasing* trend of HCl adsorption in going from pure HCl to HCl in the presence of H<sub>2</sub>O (going from black to blue in Fig. 2) may be interpreted as a displacement process: H<sub>2</sub>O displaces already adsorbed HCl, thereby reducing the adsorption capacity of HCl in the presence of H<sub>2</sub>O.

This result seems in some way to be contradictory to the values of the Langmuir constants  $K_L$  displayed in Table 2. The obtained H<sub>2</sub>O and HCl adsorption data are sufficient for the interpretation of HCl kinetics in the present work; however, they only lead to a speculative interpretation of the HCl and H<sub>2</sub>O adsorption data for the moment. We will refrain from a molecular interpretation until additional data on this system have been obtained.

Langmuir isotherms are not the only isotherms used to describe surface adsorption. For instance, Deitz and Turner (1970) used conventional Type II physical adsorption isotherms to describe the adsorption of water on the walls of a glass–Kovar stainless steel vacuum system in the pressure range from 0.2 to 5 Torr. Type II isotherms are also known as BET (Brunauer–Emmett–Teller) adsorption isotherms and allow for multilayer adsorption in contrast to simple Langmuir theory (Gregg and Sing, 1982). They conclude that the water adsorption strongly depends on the materials and needs to be determined for each apparatus. On the other hand, electrochemical quartz crystal microbalance measurements have been used to determine the adsorption of fission products (caesium and iodide) in their ionic form on the surface of stainless steel and zirconium (Repanszki et al., 2007). The authors conclude that a Langmuir-type isotherm is able to describe the adsorption, where the saturation values correspond to surface monolayers.

Furthermore, Langmuir adsorption models have also been successfully used to describe sub-monolayer adsorption of organics (Winkler et al., 2002; von Hessberg et al., 2008) as well as inorganics on ice (Pouvesle et al., 2010). Recently, experiments monitoring the density of adsorbed acetone molecules on ice using a combination of X-ray photoemission spectroscopy (XPS) and near-edge X-ray absorption spectroscopy (NEXAFS) have been performed where results have been expressed in terms of Langmuir adsorption isotherms (Starr et al., 2011).

## 5.2 Mass balance and stoichiometry

When introduced into the SFR at low temperatures in the presence of ice, a molecule of X may follow one of three different pathways: it may effuse out of the reactor through the leak valve; it may be adsorbed onto the walls of the reactor; or it may condense onto the low temperature ice. Namely, if  $N_{in}(X)$  is the number of molecules introduced into the reactor, we have  $N_{in}(X) = N_{esc}(X) + N_{ads}(X) + N_{HH}(X)$ , where  $N_{esc}(X)$  is the number of molecules of X that effuse out of the chamber,  $N_{ads}(X)$  the molecules adsorbed onto the internal walls of the reactor and  $N_{HH}(X)$  is the number of molecules in the condensed ice phase.

$N_{in}(X)$  is measured by means of the pressure drop in a calibrated volume,  $N_{esc}(X)$  corresponds to the integral over time of the calibrated MS signal and  $N_{ads}(X)$  may be calculated according to Eq. (7) using the measured equilibrium constant

$K_L$ .  $N_{HH}(X)$  is calculated using a mass balance argument as the difference  $N_{HH}(X) = N_{in}(X) - (N_{ads}(X) + N_{esc}(X))$ .

We may also calculate  $N_{FTIR}(X)$  in the case of HCl as follows: using the measured optical density at 1635 cm<sup>-1</sup> and the known IR cross section at the same frequency, namely  $\sigma = (6.5 \pm 1.9) \times 10^{-19}$  cm<sup>2</sup> (Chiesa and Rossi, 2013), the number of HCl molecules in the condensed phase may be calculated according to Eq. (12):

$$N_{FTIR}(HCl) = \frac{\ln(10) \cdot OD^{1635}}{\sigma} \cdot A_{Si}, \quad (12)$$

where OD is the optical density in absorbance units,  $A_{Si}$  the area (one side) of the silicon film support and  $\sigma$  is the IR absorption cross section at 1635 cm<sup>-1</sup>, respectively. Making use of the multidagnostic capabilities of the system, we may therefore establish a mass balance of molecules in the condensed phase between  $N_{HH}(HCl)$  and  $N_{FTIR}(HCl)$ . Table 3 lists the contributing terms as well as the comparison between  $N_{HH}(HCl)$  and  $N_{FTIR}(HCl)$ .

Similarly, for H<sub>2</sub>O, the number of molecules of H<sub>2</sub>O in the condensed phase,  $N_{FTIR}(H_2O)$ , may be calculated according to Eq. (13):

$$N_{FTIR}(H_2O) = \frac{\ln(10) \cdot OD^{3233}}{\sigma} \cdot A_{Si}, \quad (13)$$

where  $\sigma = (8.0 \pm 0.8) \times 10^{-19}$  cm<sup>2</sup> (Chiesa and Rossi, 2013) is the IR absorption cross section of pure ice at 3233 cm<sup>-1</sup>.

Equations (12) and (13) may be used to determine the stoichiometry of the condensed phase. Upon formation of HH during exposure of HCl, the peak intensity at 3233 cm<sup>-1</sup> decreases. The decrease in OD may be used to calculate the number of H<sub>2</sub>O molecules that are used to construct the new crystalline HCl · 6H<sub>2</sub>O phase. The number of available H<sub>2</sub>O is given by the total number of H<sub>2</sub>O in the pure ice film before HCl exposure and calculated according to Eq. (13). After the HCl exposure to the ice film had been halted, the deconvolution procedure described in Sect. 4.3 has been applied to the composite spectrum of the film at steady-state conditions. The resulting spectrum for the excess water (blue spectrum in Fig. S4 in the Supplement) is then used to calculate the number of pure H<sub>2</sub>O in the sample that are not associated with HCl, according to Eq. (13). The number of HCl molecules in the sample, namely  $N_{FTIR}(HCl)$ , is calculated according to Eq. (12).

Equivalently, the same information on  $N_{FTIR}(HCl)$  may be obtained in the following procedure and is called  $N_{HH}(H_2O)$ . The decrease in OD at 3233 cm<sup>-1</sup>,  $\Delta(OD)$ , yields the difference between  $N_{pure}(H_2O)$ , the number of H<sub>2</sub>O molecules in the initially pure ice film, and  $N_{ice}(H_2O)$ , the number of H<sub>2</sub>O molecules in excess pure ice of the doped sample that is not involved in forming crystalline HH absorbing at 3233 cm<sup>-1</sup>, the frequency of pure ice absorption.  $\Delta(OD)$  leads to the number of H<sub>2</sub>O molecules that have been used to construct the HH phase, namely  $N_{HH}(H_2O)$ , according to Eq. (13)

**Table 3.** Mass balance and stoichiometry for selected experiments on HCl crystalline hexahydrates.

HCl					
Exp	$N_{\text{in}}(\text{HCl})$ [molec] $\times 10^{17}$	$N_{\text{esc}}(\text{HCl})$ [molec] $\times 10^{17}$	$N_{\text{ads}}(\text{HCl})$ [molec] $\times 10^{16}$	$N_{\text{HH}}(\text{HCl})$ [molec] $\times 10^{17}$	$N_{\text{FTIR}}(\text{HCl})$ [molec] $\times 10^{17}$
1	5.19 $\pm$ 0.26	1.18 $\pm$ 0.06	6.73 $\pm$ 0.34	3.34 $\pm$ 0.17	2.94 $\pm$ 0.86
2	6.00 $\pm$ 0.30	1.28 $\pm$ 0.06	9.99 $\pm$ 0.50	3.72 $\pm$ 0.19	3.27 $\pm$ 0.96
3	6.09 $\pm$ 0.30	1.19 $\pm$ 0.06	7.78 $\pm$ 0.39	4.12 $\pm$ 0.21	3.14 $\pm$ 0.92
4	5.48 $\pm$ 0.49	1.04 $\pm$ 0.05	6.31 $\pm$ 0.32	3.81 $\pm$ 0.19	2.92 $\pm$ 0.85
5	4.79 $\pm$ 0.24	0.79 $\pm$ 0.04	8.95 $\pm$ 0.45	3.11 $\pm$ 0.16	3.05 $\pm$ 0.89
H <sub>2</sub> O					
Exp	$N_{\text{pure}}(\text{H}_2\text{O})$ [molec] $\times 10^{18}$	$N_{\text{ice}}(\text{H}_2\text{O})$ [molec] $\times 10^{18}$	$N_{\text{HH}}(\text{H}_2\text{O})$ [molec] $\times 10^{18}$	$R_{\text{HH}}^{\text{a}}$	$S_{\text{HH}}^{\text{b}}$
1	4.89 $\pm$ 0.24	3.16 $\pm$ 0.16	1.73 $\pm$ 0.09	1.14	5.89
2	4.78 $\pm$ 0.24	2.68 $\pm$ 0.13	2.10 $\pm$ 0.11	1.14	6.42
3	5.03 $\pm$ 0.25	3.17 $\pm$ 0.16	1.86 $\pm$ 0.09	1.31	5.93
4	4.72 $\pm$ 0.24	3.42 $\pm$ 0.17	1.31 $\pm$ 0.07	1.30	4.47
5	3.77 $\pm$ 0.19	1.82 $\pm$ 0.09	1.95 $\pm$ 0.10	1.02	6.39

<sup>a</sup> The mass balance ratio  $R_{\text{HH}}(\text{HCl})$  is given by  $N_{\text{HH}}(\text{HCl})/N_{\text{FTIR}}(\text{HCl})$ .

<sup>b</sup> The average stoichiometric ratio  $S_{\text{HH}} = N_{\text{HH}}(\text{H}_2\text{O})/N_{\text{FTIR}}(\text{HCl})$  is  $5.80 \pm 0.70$  taking into account all experiments. Excluding the outlier of 4.47 leads to an average ratio of  $6.16 \pm 0.29$ .

and Table 3. Finally, the ratio  $S_{\text{HH}} = N_{\text{HH}}(\text{H}_2\text{O})/N_{\text{FTIR}}(\text{HCl})$  reveals the stoichiometry of the crystalline film leading to H<sub>2</sub>O : HCl = 6 : 1 reported in Table 3.

Table 3 shows results for all experiments performed. In all cases the HCl mass balance ratio  $R_{\text{HH}} = N_{\text{HH}}(\text{HCl})/N_{\text{FTIR}}(\text{HCl})$  and the stoichiometric ratio  $S_{\text{HH}} = N_{\text{HH}}(\text{H}_2\text{O})/N_{\text{FTIR}}(\text{HCl})$  of the condensed phase have been calculated at the end of the HH growth protocol, once steady-state conditions had been reached and before PV dosing experiments began. The HCl mass balance ratio yields an average value of  $1.18 \pm 0.12$ . The wall-adsorbed molecules account for about 12 to 19 % of the total number of molecules let into the reactor and for about 22 to 30 % of the number of molecules adsorbed onto the ice. These results show that particular caution has to be exercised in the description of the gas–wall interaction in the SFR due to the importance it has in the processes involved. The measured stoichiometric ratio yields an average value of  $5.8 \pm 0.7$ , in agreement with the expected value of 6.00 for HCl · 6H<sub>2</sub>O. If we regard experiment 4 as an outlier because it is barely inside the  $2\sigma$  interval, we obtain an average value for the stoichiometry of the crystalline phase of  $6.2 \pm 0.3$ , remarkably close to the expected theoretical value considering the experimental uncertainty.

### 5.3 HCl/H<sub>2</sub>O phase diagram

As described in Sect. 4.3, the deconvolution procedure shown in Fig. 7 leads to observable HCl hexahydrate concentrations for all experiments conducted outside the known HH existence area. They all pertain to binary HH–ice films,

and we, therefore, propose extending the existence area of HCl · 6H<sub>2</sub>O by modifying the HCl/H<sub>2</sub>O phase diagram to include the present results, as shown in Fig. 8 by the shaded area. We preserve the slope of the coexistence line of hexahydrate and trihydrate as calculated by Wooldridge et al. (1995) and simply apply a parallel displacement of the phase boundary whose slope depends on the stoichiometry of the two hydrates and their enthalpies of sublimation.

Figure 9a shows the phase diagram as a function of the equilibrium vapour pressures  $P_{\text{eq}}(\text{H}_2\text{O})$  and  $P_{\text{eq}}(\text{HCl})$ , reconstructed from Hanson and Mauersberger (1990). The empty triangles represent the calculated values of  $P_{\text{eq}}(\text{H}_2\text{O})$  and  $P_{\text{eq}}(\text{HCl})$  for HH using the kinetic results for adsorption and desorption obtained from the present work, according to Eq. (11). The proposed extension of the HH existence area is represented as well. The quadruple points remain and are not affected by the additional data. Figure 9b shows an example of two experiments as a time series when the temperature of the ice substrate is increased in the range 167 to 197 K. Both experiments have been performed as described in Sect. 3.3.

Before describing the two experiments represented by red and purple lines (Fig. 9b), it is important to understand the behaviour of a sample in a simpler case. We will follow the black dotted line labelled “180 K” in Fig. 9a, which represents the isotherm at temperature  $T = 180$  K. Along this line,  $P_{\text{eq}}(\text{HCl})$  may be increased up to approximately  $2.5 \times 10^{-7}$  Torr with no detectable change in  $P_{\text{eq}}(\text{H}_2\text{O})$ . The sample behaves as pure ice even in the presence of small amounts of HCl. When the phase boundary line is reached, the phase changes from “ice” to HH. Any further increase of

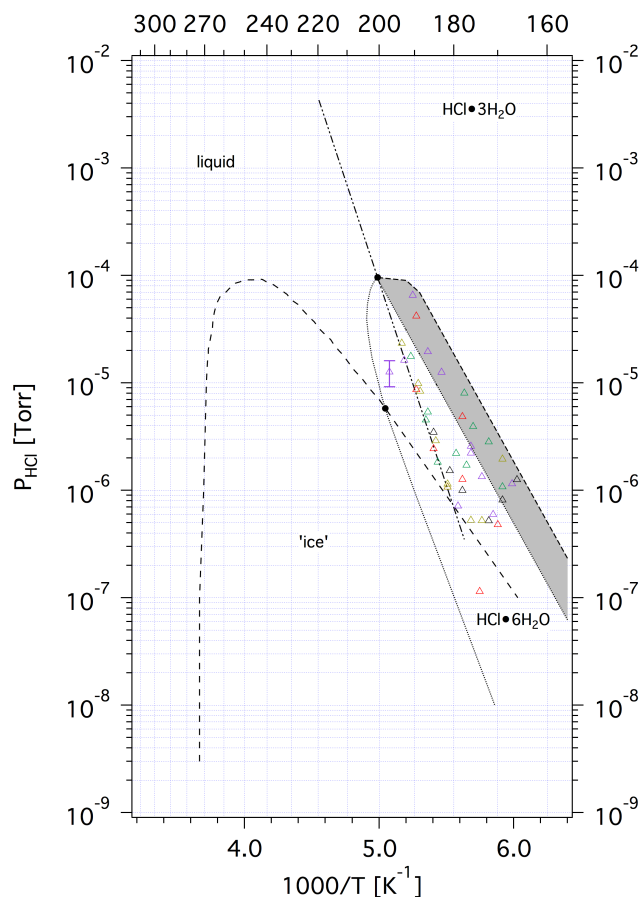


**Figure 8.** Phase diagram of the HCl/H<sub>2</sub>O system. The shaded area is the proposed extension of the HH existence area according to the results of the present work. The quadruple points (black dots) have been preserved.

$P_{\text{eq}}(\text{HCl})$  corresponds to a decrease of  $P_{\text{eq}}(\text{H}_2\text{O})$  as expected for a binary system at equilibrium following Gibbs–Duhem law, Eq. (14):

$$d\mu_{\text{HCl}} = -\frac{n_{\text{H}_2\text{O}}}{n_{\text{HCl}}} \cdot d\mu_{\text{H}_2\text{O}}, \quad (14)$$

where  $n_{\text{HCl}}$  and  $n_{\text{H}_2\text{O}}$  are the number of moles of HCl and H<sub>2</sub>O, and  $d\mu_{\text{HCl}}$  and  $d\mu_{\text{H}_2\text{O}}$  the change in chemical potential, respectively. A variation in the chemical potential of a component (HCl) in the condensed phase corresponds to the inverse variation of the chemical potential of the other component (H<sub>2</sub>O) in proportion to the stoichiometric ratio of the two components. A large variation of  $P_{\text{eq}}(\text{HCl})$  is allowed along an isotherm compared to a much smaller variation of  $P_{\text{eq}}(\text{H}_2\text{O})$ .

As HCl increases along the isotherm,  $P_{\text{eq}}(\text{H}_2\text{O})$  decreases until the boundary line between hexahydrate and trihydrate is reached and the phase changes again. The slope is less steep, reflecting the change of stoichiometry in the new solid phase. A change in temperature leads to deviations from this simple case, and the substrate may follow different paths to reach

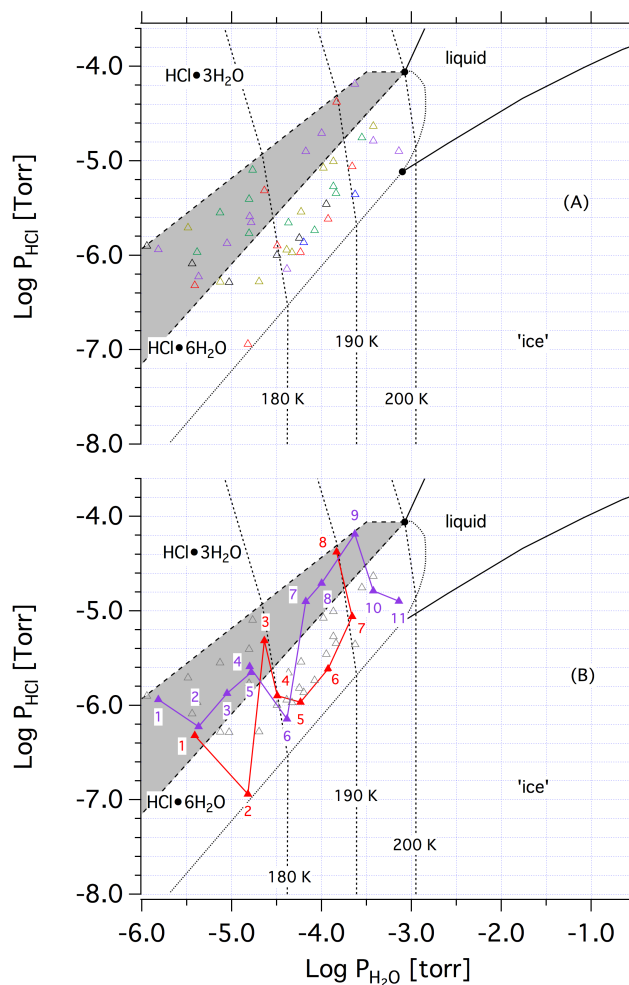


**Figure 9.** Phase diagram of the HCl/H<sub>2</sub>O system reconstructed from Hanson and Mauersberger, 1990. The empty coloured triangles represent calculated values of  $P_{\text{eq}}(\text{HCl})$  and  $P_{\text{eq}}(\text{H}_2\text{O})$  for HH using the kinetic results for adsorption and desorption of H<sub>2</sub>O and HCl of the present work, according to Eq. (11). Different colours represent different experiment series. The shaded area is the proposed extension of the HH existence area according to the results of the present work with both quadruple points preserved. **(B)** Two different experiment series where the temporal evolution of the sample is discussed. Details may be found in the text.

equilibrium. The experiments shown as red and purple lines in Fig. 9b describe the evolution of the substrate when the partial pressure of water is controlled by the introduction of an external H<sub>2</sub>O flow  $F_{\text{in}}(\text{H}_2\text{O})$  into the reactor.

First we will discuss the experiment marked in red symbols in Fig. 9b. Point 1 is the first measurement taken at 171 K. Subsequently, the temperature is increased to point 2 (175 K) while no external flow of H<sub>2</sub>O is introduced. Nevertheless, a substantial decrease in  $P_{\text{eq}}(\text{HCl})$  is observed, not only during this particular experiment but also for all experiments reported in Fig. 9a. As explained above, a decrease in  $P_{\text{eq}}(\text{HCl})$  corresponds to an increase of  $P_{\text{eq}}(\text{H}_2\text{O})$ , which

implies the presence of a flow of H<sub>2</sub>O. The water is introduced into the reactor involuntarily across numerous small air leaks owing to the presence of elastomeric seals (Viton O-rings), which add up so as to become non-negligible at these low partial pressures of H<sub>2</sub>O. The typical H<sub>2</sub>O leak rate of the reactor against the atmosphere has been checked regularly over time and found to be  $(5\text{--}10) \times 10^{-6}$  Torr l s<sup>-1</sup> in every hardware configuration used. This corresponds to an air flow rate of  $(1.6\text{--}3.2) \times 10^{14}$  molec s<sup>-1</sup>. Taking a typical H<sub>2</sub>O vapour content of 3% in laboratory air at ambient temperature, we arrive at a H<sub>2</sub>O partial pressure of  $(4.3\text{--}8.6) \times 10^{-7}$  Torr in the SFR without turning on the external H<sub>2</sub>O flow. This corresponds to the equilibrium vapour pressure over pure ice at 155 to 165 K, which means that 165 K is the lower limit beyond which we cannot perform ice experiments under controlled conditions. Consistent with this fact is our observation of an increase of the thickness of the ice film due to deposition of H<sub>2</sub>O onto the ice at temperatures lower than 175 K.

From point 2 to point 3 (180 K), the temperature is increased and only a small increase in  $P_{\text{eq}}(\text{H}_2\text{O})$  is observed compared to a large increase of  $P_{\text{eq}}(\text{HCl})$ . Between point 3 and point 4,  $F_{\text{in}}(\text{H}_2\text{O})$  is introduced into the reactor at constant temperature. As a consequence  $P_{\text{eq}}(\text{HCl})$  decreases along the isotherm following the increase of  $P_{\text{eq}}(\text{H}_2\text{O})$  as expected according to Gibbs–Duhem law, Eq. (14). Both the temperature and  $F_{\text{in}}(\text{H}_2\text{O})$  are increased from point 4 to point 7 such that  $F_{\text{in}}(\text{H}_2\text{O})$  is kept approximately at  $0.1 \cdot F_{\text{ev}}(\text{H}_2\text{O})$  at any temperature. After the measurement at point 7,  $F_{\text{in}}(\text{H}_2\text{O})$  is halted and the system immediately responds to the variation of  $P_{\text{eq}}(\text{H}_2\text{O})$  by increasing  $P_{\text{eq}}(\text{HCl})$  following the isotherm at  $T = 190$  K, according to Gibbs–Duhem law, Eq. (14).

The experiment marked in purple symbols in Fig. 9b is performed in a similar way as above (red symbols) with the difference that the external flow  $F_{\text{in}}(\text{H}_2\text{O})$  is a factor of 2 lower with respect to the “red” experiment. From point 1 to point 2, we observe a drop in  $P_{\text{eq}}(\text{HCl})$  due to background H<sub>2</sub>O flow, and at point 6  $F_{\text{in}}(\text{H}_2\text{O})$  is introduced into the reactor. A lower  $F_{\text{in}}(\text{H}_2\text{O})$  leads to higher  $P_{\text{eq}}(\text{HCl})$  compared to the “red” experiment as is evident from points 7, 8 and 9 that explore the hitherto unexplored space of the HCl hexahydrate phase diagram marked as shaded area in Fig. 9. At point 10 the flow  $F_{\text{in}}(\text{H}_2\text{O})$  is increased to approximately  $0.2 \cdot F_{\text{ev}}(\text{H}_2\text{O})$  with a corresponding increase of  $P_{\text{eq}}(\text{H}_2\text{O})$  and decrease of  $P_{\text{eq}}(\text{HCl})$  along the isotherm, once again according to Gibbs–Duhem law, Eq. (14).

#### 5.4 $\alpha(\text{HCl})$ scatter and HCl hexahydrate composition

Figure 5 shows the kinetic results for HH substrate experiments. Variations in the kinetic and thermodynamic parameters up to a factor of 10 for points at the same temperatures occur. The substrate is a binary system composed of a bulk pure ice film with a thinner HH film on top of it. According to

Gibbs’ phase rule, we have  $F = C - P + 2 = 2 - 3 + 2 = 1$ , where  $F$  is the number of degrees of freedom,  $C$  the number of components, namely H<sub>2</sub>O and HCl, and  $P$  the number of phases of the system at equilibrium, namely the binary condensate, the pure ice and the gas phase. The degree of freedom of our system corresponds to the composition of the substrate, namely the mole ratio between pure ice and the HH film. Even though the growth protocol has been applied consistently to all experiments, the approach to the temperatures of interest and the exposure to transient supersaturation of gases during PV experiments, which all contribute to the “history” of the film, may lead to a different composition of the thin film at the same experimental temperature, which may explain – at least in part – the scatter of  $\alpha_{\text{ice}}(\text{HCl})$  as a function of temperature. The decrease of  $\alpha_{\text{ice}}(\text{HCl})$  in the aftermath of a pulse may also be explained as a variation of the composition of the interface, specifically the change from a H<sub>2</sub>O-rich ice film before the first pulse of HCl to a more H<sub>2</sub>O-deficient ice film when the third HCl pulse is admitted due to evaporation of H<sub>2</sub>O and accumulation of HCl.

$\alpha_{\text{ice}}(\text{H}_2\text{O})$ , on the other hand, does not present any scatter, and this may be due to the fact that the average molecular environment for H<sub>2</sub>O is constant owing to its single-component nature. In order to evaluate the ratio between pure HH and pure H<sub>2</sub>O ice, we have made use of the multidagnostic capabilities of the present system. We have selected experiments in five temperature ranges, and for each experiment we have determined the number of HH molecules using Eq. (12), and similarly the number of molecules of H<sub>2</sub>O according to Eq. (13).

The mole fraction  $\chi_{\text{H}_2\text{O}}$  of H<sub>2</sub>O in each HH film may be calculated as the ratio of the number of moles of H<sub>2</sub>O molecules to the total number of moles:

$$\chi_{\text{H}_2\text{O}} = \frac{N_{\text{H}_2\text{O}}^{\text{FTIR}}}{N_{\text{H}_2\text{O}}^{\text{FTIR}} + N_{\text{HCl}}^{\text{FTIR}}} \quad (15)$$

Figure 10 shows the results obtained for the selected experiments.  $P_{\text{eq}}(\text{HCl})$  is reported as coloured circles, whereas  $\alpha(\text{HCl})$  is presented as coloured triangles according to the temperature range. Temperature seems to have only a modest effect, whereas the history of the sample seems to have a larger impact on the film composition of every individual sample.

$P_{\text{eq}}(\text{HCl})$  increases as the concentration of HCl in the film increases, as expected, according to the change in chemical potential in the binary system.  $\alpha(\text{HCl})$  decreases as excess H<sub>2</sub>O evaporates, and the concentration of HCl increases accordingly because the faster H<sub>2</sub>O evaporation compared to HCl leads to a situation where decreasing amounts of H<sub>2</sub>O are available in the condensate to accommodate the HCl molecules in the gas phase that hit the ice surface.

At high HCl concentration and OD at  $3233 \text{ cm}^{-1}$  lower than 0.15 absorbance units, which is when the film thickness is less than  $0.15 \mu\text{m}$ , we observe a decrease of  $R_{\text{ev}}(\text{H}_2\text{O})$  as

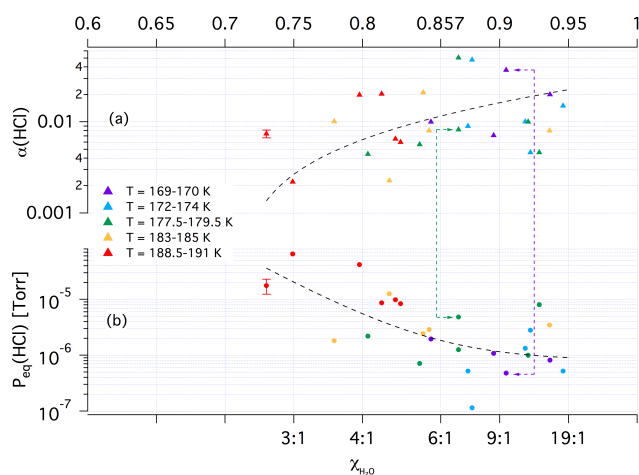


**Figure 10.**  $P_{\text{eq}}(\text{HCl})$  and  $\alpha(\text{HCl})$  as a function of mole fraction of H<sub>2</sub>O in HH film. The bottom and top axes indicate the H<sub>2</sub>O : HCl ratio and the H<sub>2</sub>O weight percentage in the film, respectively. Colours identify different temperature ranges, and the broken lines just serve to guide the eye. Coloured arrows indicate an example of pairs of data points.

well as an increase of  $R_{\text{ev}}(\text{HCl})$  in agreement with Chiesa and Rossi (2013) and Delval et al. (2003). This is an indication of a phase change, namely the conversion of HH into an amorphous mixture of higher HCl : H<sub>2</sub>O ratio.

Nevertheless, the composition of the HH film cannot completely explain the scatter in the values of  $\alpha(\text{HCl})$  and  $P_{\text{eq}}(\text{HCl})$  such as displayed in Fig. 5. McNeill et al. (2007) have observed variations up to a factor of 3 for the HCl partial pressure of smooth ice samples exposed to HCl vapour after HH formation, and they have explained these variations in terms of surface roughness and surface disorder of the ice substrates. The scatter in our results may also be due in part to surface morphology variations or inhomogeneities of the film surface of each sample. The ice sample is repeatedly exposed to a high supersaturation of HCl during PV experiments, and this may lead to surface liquefaction and/or reconstruction coupled to concentration changes of the surface components compared to bulk composition in comparison to the explanation given by McNeill et al. (2007). In addition, the pioneering and superb work of Kuhs et al. (2012) on the structure of ice in terms of stacking faults of hexagonal ice  $I_{\text{h}}$  masquerading as “cubic” ice  $I_{\text{c}}$  has to be considered when investigating chemical reactions involving the evaporation and condensation of H<sub>2</sub>O in pure and doped ices. As a consequence every reaction on and within ice, including the present thin ice films, has to be evaluated in terms of the “natural” (i.e. spontaneous) conversion of “cubic” ice to its thermodynamically stable counterpart  $I_{\text{h}}$ . As a result, one cannot be sure that laboratory-grown ice samples exclusively consist of pure stable ice  $I_{\text{h}}$  or a mixture mimicking the unstable, but more reactive phase  $I_{\text{c}}$ , without prior in-depth investiga-

tion of its structure. It may be that many previous laboratory investigations may have to be reevaluated in that respect.

### 5.5 Composition of amorphous phase

In order to provide an estimate of the composition of the amHCl substrates, we compared the present spectra with the ones from Xueref and Dominé (2003). In their work the authors grew doped ice films by co-condensation of gaseous mixtures HCl/H<sub>2</sub>O of 5 : 1, 1 : 10, 1 : 50 and 1 : 200 composition at 190 K. The condensation of the 5 : 1 mixture leads to a solid that resembles HCl · 2H<sub>2</sub>O where partial crystallization takes place, whereas the condensation of gaseous mixtures of HCl : H<sub>2</sub>O ratios of 1 : 10, 1 : 50 and 1 : 200 leads to the formation of non-crystalline solids whenever there is excess H<sub>2</sub>O. In particular, the 1 : 10 gaseous mixture leads to a solid of composition in the range 1 : 2 to 1 : 4 regarding HCl : H<sub>2</sub>O, while the 1 : 50 and 1 : 200 gaseous mixtures both lead to solids of composition in the range 1 : 4 to 1 : 6.

The above authors reason that, due to the excess of HCl incorporation in the co-condensation process, H<sub>2</sub>O and HCl are not in thermodynamic equilibrium. This may lead to the formation of a supersaturated homogenous solid solution of HCl in ice or a solid solution of HCl in ice. This may be followed by diffusion to the surface of the excess HCl and its subsequent escape into the gas phase, bringing the solution into thermodynamic equilibrium. Xueref and Dominé (2003) invoke the slightly larger HCl/ice accommodation coefficient  $\alpha(\text{HCl})$  compared to  $\alpha(\text{H}_2\text{O})$  on pure ice as the reason of HCl enrichment in the condensed phase. While this goes into the right direction, we think that this explanation is by far insufficient to rationalize the large observed enrichment factors in laboratory studies as well as in field observations on snow and ice composition. In light of the present results, we provide an additional interpretation as follows: the higher  $R_{\text{ev}}(\text{H}_2\text{O})$  compared to  $R_{\text{ev}}(\text{HCl})$  leads to rapid evaporation of water from the forming ice sample that is 2 orders of magnitude larger than HCl, as shown in Fig. 3. This large difference between  $R_{\text{ev}}(\text{H}_2\text{O})$  and  $R_{\text{ev}}(\text{HCl})$  effectively explains the large enrichment of HCl in the condensed phase (ice) despite the large atmospheric abundance of H<sub>2</sub>O vapour over HCl extending over several orders of magnitude. The fact that the present results have been obtained at temperatures much lower than typical snow sampling data does not change the conclusions because the ratio of the HCl and H<sub>2</sub>O evaporation rates changes only little from 190 to 250 K.

In the present case we grew amHCl film by exposing a pure ice film of thickness in the range 1 to 2  $\mu\text{m}$  ( $3$  to  $6 \times 10^{18}$  molecules) to a total dose of approximately  $3 \times 10^{17}$  molecules of HCl at 175 K. Our samples are therefore a superposition of a bulk pure ice film with an amHCl film on top of it. As the abundance of H<sub>2</sub>O decreases in the film, the spectroscopic characteristics of the film change as well, as presented in Fig. 11, where the temporal evolution of an amHCl film is shown under SFR conditions. A pure ice

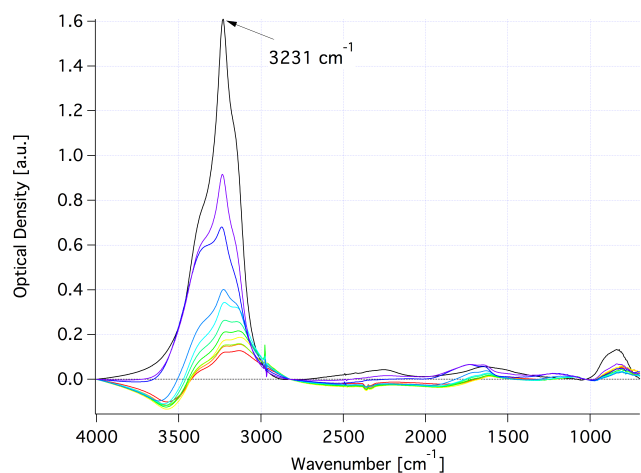


**Figure 11.** Evolution of amHCl film: the spectrum of a pure ice film is represented in black, and the conversion of an amHCl from a H<sub>2</sub>O-rich film (purple spectrum) to an amorphous HCl-ice film (red spectrum) while pumping under SFR is displayed in colour. The spectra are colour-coded as a function of temperature in the range 175 to 200 K, with each spectrum corresponding to a temperature increase of roughly 3 K. All spectra from blue to red have been measured in the aftermath of the first pulse in a series of consecutive PV experiments. A constant flow of HCl has been used in going from black (pure ice) to purple.

film (black spectrum) at 175 K is exposed to a flow of HCl of  $1 \times 10^{15}$  molec s<sup>-1</sup> for roughly 10 min. Upon halting the HCl flow, the following spectral changes (purple spectrum) appear: a drastic decrease of the peak amplitude at 3233 cm<sup>-1</sup> as well as an increasing shoulder at 3400 cm<sup>-1</sup> and a broad band at 1700 cm<sup>-1</sup> owing to the deposition of HCl. When deposition is halted, the desired temperature for PV experiments is set. The spectrum continues to change even after the halt of the HCl flow, showing a further decrease of the peak at 3233 cm<sup>-1</sup> (blue spectrum) in the aftermath of the first pulse of an HCl PV series at 175 K. As the temperature increases from 175 to 200 K, more excess H<sub>2</sub>O evaporates and the film loses the characteristic peak of pure ice at 3233 cm<sup>-1</sup> and converts to a complete amorphous HCl/H<sub>2</sub>O mixture film as shown by the red spectrum, albeit at lower amplitude owing to evaporation of HCl and H<sub>2</sub>O.

In Fig. 12 we have compared the complete amHCl films from Fig. 11 in the temperature range 187 to 200 K with the spectra recorded by Xueref and Dominé (2003). We only considered the spectra for the HCl/H<sub>2</sub>O gaseous mixtures of ratios 1 : 200 (black line) and 1 : 50 (grey line) as these are the spectra that come closest to the expected composition of the present samples. Indeed, this is the case since all spectra are fairly similar. It therefore appears that all the present samples, once the excess H<sub>2</sub>O has evaporated, are in the composition range 1 : 4 to 1 : 6 of HCl : H<sub>2</sub>O.

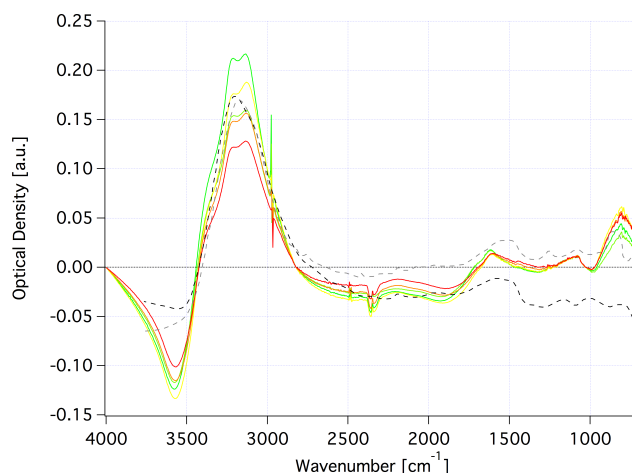


**Figure 12.** Comparison of FTIR spectra of amHCl films. Our experimentally measured spectra are shown in colours according to temperature, whereas the dashed spectra correspond to samples made by condensing HCl/H<sub>2</sub>O gaseous mixtures of ratios 1 : 200 (black line) and 1 : 50 (grey line) at 190 K of Xueref and Dominé (2003). The temperature of the ice sample ranges between 187 and 200 K with each spectrum measured in the aftermath of the first pulse in a series of PV experiments at temperature intervals of roughly 3 K.

## 5.6 Kinetic and thermodynamic aspects of HCl/H<sub>2</sub>O phase diagram

The progress that the present work represents over a similar recent investigation into the HCl · 6H<sub>2</sub>O vs. the amorphous HCl/H<sub>2</sub>O phase lies in the thermochemical closure of the measured accommodation and evaporation kinetics of X in the presence of pure ice with the measured partial pressure of species X of the binary system X = HCl, H<sub>2</sub>O. In other words, independent measurements of both  $\alpha(X)$  and  $R_{ev}(X)$  lead to the equilibrium vapour pressure  $P_{eq}(X)$  given by the ratio  $R_{ev}(X)/\alpha(X)$ , which subsequently may be compared with independently measured values of  $P_{eq}(X)$  from other sources. This comparison in an overdetermined system is an excellent test of the self-consistency of the kinetic with the corresponding thermochemical parameters. At least for H<sub>2</sub>O Figs. 3a and 5a provide good examples of the thermochemical consistency of the present data, both for pure ice (Marti and Mauersberger, 1993) as well as for HCl · 6H<sub>2</sub>O and amHCl/H<sub>2</sub>O whose equilibrium vapour pressures are close to the ones for pure ice (Hanson and Mauersberger, 1990).

Figure 13a and b display both an Arrhenius plot of  $J_{ev}(HCl)$  and van't Hoff plot of  $P_{eq}(HCl)$  for the interaction of HCl with amHCl/H<sub>2</sub>O in comparison with results of an earlier Knudsen flow reactor study at steady-state addressing a slightly different region of the HCl/H<sub>2</sub>O phase diagram, namely the HCl/H<sub>2</sub>O liquid-ice coexistence region (Flückiger et al., 1998; Chiesa and Rossi, 2013). The following equations define the corresponding straight lines based

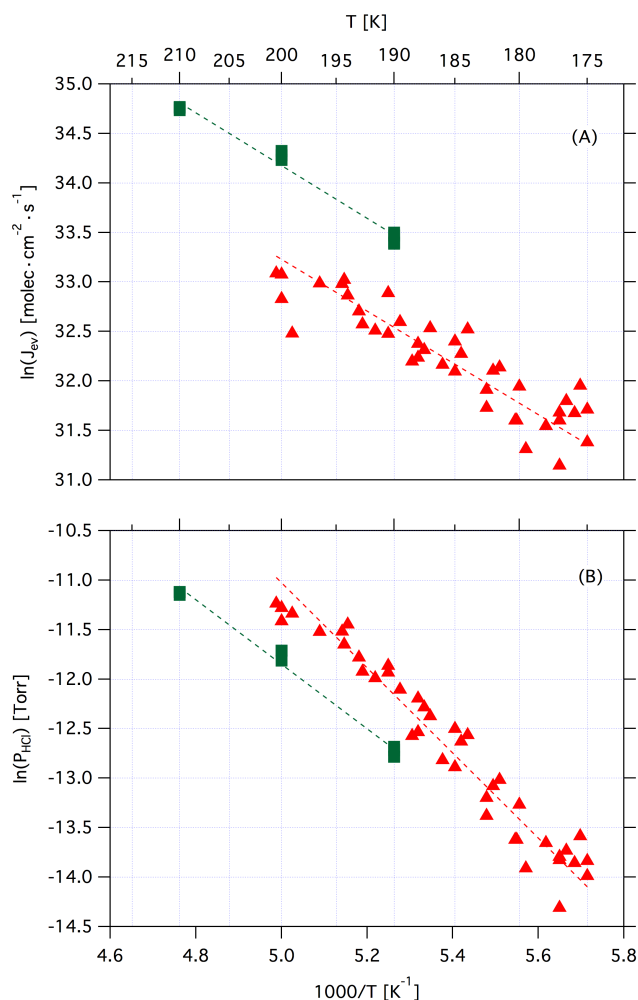


**Figure 13.** Arrhenius plot of  $J_{\text{ev}}(\text{HCl})$  (A) and van't Hoff plot of  $P_{\text{eq}}(\text{HCl})$  (B). Red triangles represent the results for the interaction of HCl with amHCl/H<sub>2</sub>O down to T = 175 K (this study) and green squares the results from a Knudsen flow reactor study addressing the HCl/H<sub>2</sub>O liquid–ice coexistence region (Flückiger et al., 1998). The equations for the fitting lines may be found in the text.

on the present ( $V/S = 1028.3 \text{ cm}$ ) as well as literature measurements (Flückiger et al., 1998;  $V/S = 122.0 \text{ cm}$ ) taking note of the conversion of evaporation rate and flux, namely,  $R_{\text{ev}} \cdot V = J_{\text{ev}} \cdot A$  and  $R = 8.314 \text{ J K}^{-1} \text{ mol}^{-1}$ . The best linear fit for the present measurements has been calculated using the iterative Levenberg–Marquardt least orthogonal distance method, which minimizes the orthogonal distance of each point from the line of best fit. For the amHCl/H<sub>2</sub>O region (Eqs. 16 and 17) and ice–liquid coexistence line (Eqs. 18 and 19), we find the following results:

$$\begin{aligned} \log J_{\text{ev}}(\text{HCl}) [\text{cm}^{-2} \text{s}^{-1}] & \quad (16) \\ & = (20.11 \pm 0.46) - (21.73 \pm 1.63) \times 10^3 / (2.303 \cdot RT) \end{aligned}$$

$$\begin{aligned} \log P_{\text{eq}}(\text{HCl}) [\text{Torr}] & \quad (17) \\ & = (4.55 \pm 0.39) - (35.76 \pm 1.38) \times 10^3 / (2.303 \cdot RT) \end{aligned}$$

$$\begin{aligned} \log J_{\text{ev}}(\text{HCl}) [\text{cm}^{-2} \text{s}^{-1}] & \quad (18) \\ & = (20.62 \pm 0.29) - (22.11 \pm 1.09) \times 10^3 / (2.303 \cdot RT) \end{aligned}$$

$$\begin{aligned} \log P_{\text{eq}}(\text{HCl}) [\text{Torr}] & \quad (19) \\ & = (1.92 \pm 0.29) - (27.05 \pm 1.11) \times 10^3 / (2.303 \cdot RT). \end{aligned}$$

$J_{\text{ev}}(\text{HCl})$  for amHCl/H<sub>2</sub>O (red triangles) resulting from the present work is a factor of 2.6 smaller than for HCl adsorbed on ice either in the HCl/H<sub>2</sub>O liquid phase or the H<sub>2</sub>O–ice coexistence line as displayed by green squares in Fig. 13a.  $J_{\text{ev}}(\text{HCl})$  values for both of these slightly different areas of the phase diagram have been found to be identical (Flückiger et al., 1998). The kinetic results indicate that the slopes of both straight lines displayed in Fig. 13a corresponding to the activation energy for HCl evaporation are identical within the given uncertainties, namely  $21.7 \pm 1.6$  (this work, Eq. 16) and  $22.1 \pm 1.1 \text{ kJ mol}^{-1}$  (Flückiger et al., 1998, Eq. 18). Although the evaporation process is identical in both cases, it suggests that some structural or compositional parameters such as the abundance of H<sub>2</sub>O on the surface must be different in both cases, thus accounting for the significant difference in the absolute values of  $J_{\text{ev}}(\text{HCl})$ , Eqs. (16) vs. (18). The corresponding equilibrium vapour pressures  $P_{\text{eq}}(\text{HCl}) = R_{\text{ev}}(\text{HCl})/\alpha(\text{HCl})$ , Eqs. (17) and (19), are in agreement with the published phase diagram (Molina, 1994) and point to a slightly higher value of the present data for amHCl/H<sub>2</sub>O ( $\Delta H_{\text{ev}}^0(\text{HCl}) = 35.8 \pm 1.4 \text{ kJ mol}^{-1}$ ) compared to the Flückiger data ( $\Delta H_{\text{ev}}^0(\text{HCl}) = 27.1 \pm 1.1 \text{ kJ mol}^{-1}$ ) pertaining to the HCl/H<sub>2</sub>O liquid–ice coexistence line. Naively, one may think that the slightly higher value of  $\Delta H_{\text{ev}}(\text{HCl})$  of the present work suggests a slightly lower HCl concentration, i.e. slightly more diluted solution of the amHCl/H<sub>2</sub>O of the present work compared to the Flückiger data on the basis of the data on HCl standard heats of solution ( $\Delta H_{\text{soln}}^0(\text{HCl})$ ) given in Wagman et al. (1982).

However, one would expect a slightly larger absolute value for  $\Delta H_{\text{soln}}^0(\text{HCl})$  for the HCl/H<sub>2</sub>O liquid–ice coexistence line compared to amHCl/H<sub>2</sub>O. The caveat is that the thermodynamic interpretation of the slopes in terms of  $\Delta H_{\text{ev}}^0$  is not feasible because the coexistence line is the end point of a family of different HCl isoconcentration lines of the liquid domain at different temperatures. However, a thermodynamic value may be determined from the difference of activation energies for the evaporation ( $E_{\text{ev}}$ , Eq. 18) and accommodation ( $E_{\text{acc}}$ ) rate of HCl on ice measured by Flückiger et al. (1998) and is calculated as  $\Delta H_{\text{ev}}^0 = \Delta H_{\text{soln}}^0(\text{HCl}) = 22.11 - (-7.53) = 29.64 \text{ kJ mol}^{-1}$  (Flückiger et al., 1998). This value is slightly larger than that given in Eq. (19).

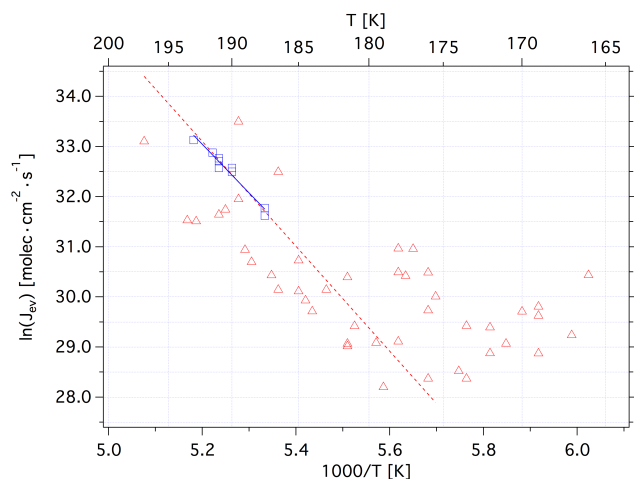


**Figure 14.** Arrhenius plot of  $J_{\text{ev}}(\text{HCl})$  for  $\text{HCl} \cdot 6\text{H}_2\text{O}$ . Red triangles represent the results of this study and blue squares the results of Chiesa and Rossi (2013) obtained from the decay of crystalline  $\text{HCl} \cdot 6\text{H}_2\text{O}$ . The equations for the linear fits may be found in the text.

This value closely corresponds to  $\Delta H_{\text{ev}}^0$  of a 1 : 1 = HCl : H<sub>2</sub>O concentrated aqueous solution ending up on the ice–liquid coexistence line of the HCl/H<sub>2</sub>O phase diagram (Wagman et al., 1982). When addressing the liquid domain of the phase diagram, Flückiger obtained  $E_{\text{ev}}$  identical to the above value to  $E_{\text{acc}}$  measured as  $-12.97 \text{ kJ mol}^{-1}$  such that  $\Delta H_{\text{ev}}^0(\text{HCl}) = \Delta H_{\text{soln}}^0(\text{HCl}) = 22.11 - (-12.97) = 35.08 \text{ kJ mol}^{-1}$  was obtained, which compares favourably with the exponential term of Eq. (11), namely  $\Delta H_{\text{ev}}^0(\text{HCl}) = 35.76 \pm 1.38 \text{ kJ mol}^{-1}$ .

Figure 14 presents an Arrhenius plot of  $J_{\text{ev}}(\text{HCl})$  of the crystalline phase over an extended temperature range that greatly exceeds the range covered by Chiesa and Rossi (2013) in their work on the decay of  $\text{HCl} \cdot 6\text{H}_2\text{O}$  by following the IR absorption specific to the metastable hydrate at  $3426 \text{ cm}^{-1}$ . Equation (20) presents the two-parameter representation of the Arrhenius line ( $J_{\text{ev}}(\text{HCl})$ ) for crystalline  $\text{HCl} \cdot 6\text{H}_2\text{O}$ , and Eq. (21) recalls the Arrhenius line of Chiesa and Rossi (2013) using  $V/A = 1506.4 \text{ cm}$ :

$$\log J_{\text{ev}}(\text{HCl}) [\text{cm}^{-2} \text{s}^{-1}] = (38.02 \pm 4.82) - (87.03 \pm 16.96) \times 10^3 / (2.303 \cdot RT) \quad (20)$$

$$\log J_{\text{ev}}(\text{HCl}) [\text{cm}^{-2} \text{s}^{-1}] = (36.31 \pm 1.65) - (80.83 \pm 6.01) \times 10^3 / (2.303 \cdot RT) \quad (21)$$

A look at Fig. 14 reveals considerable scatter of the data of the Arrhenius plot, which covers a fairly substantial temperature range compared to the Chiesa and Rossi (2013) data. The possible reasons for this scatter have been discussed above in the context of the kinetic parameters of  $\text{HCl} \cdot 6\text{H}_2\text{O}$ . This is reflected in the significant uncertainties of Eq. (20) compared to the work of Chiesa and Rossi (2013) despite the narrow

temperature range covered in that work. Considering these differences the agreement between both data sets is seen to be very good so that we conclude that the rate-limiting step in the decay of  $\text{HCl} \cdot 6\text{H}_2\text{O}$  is HCl evaporation, akin to the conclusions by Chiesa and Rossi (2013). This agreement between both methods is quite satisfying given the fact that Chiesa and Rossi followed the destruction of the condensed phase, whereas the present work is conducted by observing the behaviour of the gas phase in the presence of  $\text{HCl} \cdot 6\text{H}_2\text{O}$ .

A closer look at the data of Fig. 14 reveals that the observed positive  $T$  dependence of HCl evaporation may turn into a negative  $T$  dependence for  $T < 172 \pm 2 \text{ K}$ , which is the limit between the stable and metastable domain of  $\text{HCl} \cdot 6\text{H}_2\text{O}$  (Chiesa and Rossi, 2013). It is possible that the limit of thermodynamic stability is in some way connected to the turnover in the  $T$  dependence of the rate of HCl evaporation  $R_{\text{ev}}(\text{HCl})$  of  $\text{HCl} \cdot 6\text{H}_2\text{O}$ .

However, we are rapidly leaving the temperature range of atmospheric interest. The comparison between  $E_{\text{ev}}(\text{HCl})$  in  $\text{HCl} \cdot 6\text{H}_2\text{O}$  of approximately  $87.0 \pm 17.0 \text{ kJ mol}^{-1}$  following Eq. (14) has to be contrasted with the standard heat of sublimation of HCl calculated by Wooldridge et al. (1995) of  $65.8 \text{ kJ mol}^{-1}$  at 200 K according to Reaction (R28), which, however, does *not* correspond to the usual definition of the standard heat of sublimation of a compound because H<sub>2</sub>O stays in the condensed phase:



This leads to an activation energy  $E_{\text{ad}}$  of HCl insertion or adsorption, the inverse process of Reaction (R11), of  $E_{\text{ad}} = (87 \pm 17) - 65.8 = 21.2 \pm 17.0 \text{ kJ mol}^{-1}$ , a decidedly positive activation energy in contrast to most other adsorption processes presented in this work. This peculiarity of an intrinsic positive activation energy for the inverse process has already been mentioned by Chiesa and Rossi (2013) and may have to do with the high value of activation energy  $E_{\text{ev}}(\text{HCl})$  out of the crystalline environment of  $\text{HCl} \cdot 6\text{H}_2\text{O}$ . In contrast, the corresponding activation energy  $E_{\text{ad}}$  for the case of the amorphous liquid is calculated as  $E_{\text{ad}} = 21.7 - 35.8 = -14.1 \text{ kJ mol}^{-1}$  using Eqs. (16) and (17), which is expected behaviour for this type of process.

Finally, a comparison between the absolute value of  $E_{\text{ev}}$  of the amHCl/H<sub>2</sub>O (Eq. 16) and  $\text{HCl} \cdot 6\text{H}_2\text{O}$  (Eq. 20) may be considered. It is intuitively clear that HCl, which is surrounded by H<sub>2</sub>O molecules in a crystalline, albeit metastable hydrate shell may be more difficult to evaporate than HCl, either dissolved in a solution or adsorbed as a non-crystalline, which is in amorphous phase. It is important to realize that the “border areas” of the “ice” solid phase containing HCl are in a disordered state (McNeill et al., 2006) and therefore do not offer a crystalline environment to HCl, at least at the interface. This means that the phase transition from the metastable crystalline ( $\text{HCl} \cdot 6\text{H}_2\text{O}$ ) to a stable phase (amHCl/H<sub>2</sub>O in both the “ice” and crystalline  $\text{HCl} \cdot 6\text{H}_2\text{O}$

phase domain) of constant composition will lead to an acceleration of  $J_{\text{ev}}(\text{HCl})$  in contrast to the situation of the equilibrium vapour pressures displayed in Fig. 13a. It is satisfying that kinetic, thermodynamic and structural properties of the relevant portions of the HCl/H<sub>2</sub>O phase diagram convey a unified physical picture based on diverse experimental methods as used by McNeill et al. (2006) and the present kinetic/thermodynamic multidagnostic investigations. Finally, we should point out that the question regarding the electrolytic dissociation of adsorbed HCl – that is, the prevalence of ionic ( $\text{H}_3\text{O}^+\text{Cl}^-$ ) vs. molecular adsorption of adsorbed HCl – has been answered in a convincing way by Parent et al. (2011), at least for temperatures up to 115 K using FTIR absorption in grazing incidence. It seems that, at temperatures typical of the UT/LS, HCl exclusively occurs in its ionic form.

### 5.7 Atmospheric implications

In this study we have confirmed the findings of Chiesa et al. (2013) that the structure of ice films (amorphous, polycrystalline,  $I_h$ ) doped with HCl is irrelevant for the nucleation and growth of  $\text{HCl} \cdot 6\text{H}_2\text{O}$ . Furthermore, in agreement with previous studies (Ritzhaupt and Devlin, 1991; Koehler et al., 1993; Henson et al., 2004; Chiesa and Rossi, 2013), we have found that  $\text{HCl} \cdot 6\text{H}_2\text{O}$  requires an HCl supersaturation of the order of 10 or higher and temperatures  $T \leq 173$  K to nucleate. Exposure of ice films to HCl at temperatures higher than 173 K invariably led to the formation of an amorphous HCl/H<sub>2</sub>O phase. The crystalline  $\text{HCl} \cdot 6\text{H}_2\text{O}$  has always been observed to convert to amorphous HCl/H<sub>2</sub>O at temperatures  $T > 193$  K under SFR conditions. On the other hand, the conversion of amorphous samples into crystalline  $\text{HCl} \cdot 6\text{H}_2\text{O}$  has never been observed under all explored experimental conditions.

On the basis of these observations, we conclude that the nucleation of  $\text{HCl} \cdot 6\text{H}_2\text{O}$  is unlikely to occur under atmospheric conditions relevant for UT/LS, where the temperatures are rarely less than 180 K. Furthermore, the high nucleation barrier for  $\text{HCl} \cdot 6\text{H}_2\text{O}$  may be the reason for its kinetic instability leading to the inability of evaporating HCl to regenerate crystalline  $\text{HCl} \cdot 6\text{H}_2\text{O}$  when it condenses back at atmospheric temperatures. The amorphous HCl/H<sub>2</sub>O phase is likely to be the relevant phase in the processes involving HCl at UT/LS atmospherically relevant conditions.

## 6 Conclusions

In this work we have gone one step further compared to our recent work on the same subject using a stirred flow reactor (Chiesa and Rossi, 2013). The improvements may be summarized as follows: (1) combination of steady-state and transient supersaturation experiments in order to measure microscopic rates of evaporation  $R_{\text{ev}}$  and accommodation  $\alpha$ ,

both for HCl and H<sub>2</sub>O interacting with crystalline HH and amorphous HCl/H<sub>2</sub>O; (2) true multidagnostic experiment addressing gas phase and condensed phase under identical reaction conditions (using FTIR absorption in transmission, we followed the gas-phase kinetics of both HCl and H<sub>2</sub>O together with the changes in the corresponding FTIR absorption spectra of the condensed phase); (3) spectral deconvolution of composite IR absorption spectra in terms of the concentration or mole fraction of HCl and H<sub>2</sub>O such that each measured point in the HCl/H<sub>2</sub>O phase diagram corresponded to a composite yet deconvoluted IR absorption spectrum.

The obtained kinetics of the forward (accommodation) and reverse (evaporation) experiments are consistent with the measured and/or previously known equilibrium vapour pressures. Among the most important experimental results that have been obtained under the constraint of thermochemical kinetics, we cite (a) HCl accommodation and evaporation kinetics are significantly slower than for H<sub>2</sub>O in the covered temperature range, both for  $\text{HCl} \cdot 6\text{H}_2\text{O}$  and the amorphous mixture of HCl/H<sub>2</sub>O. This explains the persistence of HCl in the condensed phase even under evaporation conditions. The phase transition from crystalline  $\text{HCl} \cdot 6\text{H}_2\text{O}$  to the amorphous HCl/H<sub>2</sub>O phase was controlled by the rate-limiting step of HCl rather than H<sub>2</sub>O evaporation; (b) the kinetics of HCl evaporation during the  $\text{HCl} \cdot 6\text{H}_2\text{O}$  decay measured over an extended temperature range closely corresponded to previous experiments in which the decay of the optical density of the crystalline  $\text{HCl} \cdot 6\text{H}_2\text{O}$  was recorded, albeit over a restricted temperature range; (c) as a result of using the present multidagnostic approach, we have obtained an extension of the phase diagram in the existence area of crystalline  $\text{HCl} \cdot 6\text{H}_2\text{O}$ . However, this extension leaves the two known quadruple points from previous work unchanged, as expected.

**The Supplement related to this article is available online at doi:10.5194/acp-14-5183-2014-supplement.**

*Acknowledgements.* The authors would like to acknowledge the unflinching and generous support of this work over the years by the Swiss National Science Foundation (SNSF) in the framework of projects 200020\_125204 and 200020\_144431/1. Moreover, we sincerely thank Alwin Frei for his support and patience over the years during which the experiment was located in his laboratory.

Edited by: T. Bartels-Rausch

## References

- Abbatt J. P. D., Beyer, K. D., Fucaloro, A. F., McMahon, J. R., Wooldridge, P. J., Zhang, R., and Molina, M. J.: Interaction of HCl Vapor with Water-ice: Implications for the Stratosphere, *J. Geophys. Res.* 97, 15819–15826, 1992.
- Ammann, M., Cox, R. A., Crowley, J. N., Jenkin, M. E., Mellouki, A., Rossi, M. J., Troe, J., and Wallington, T. J.: Evaluated kinetic and photochemical data for atmospheric chemistry: Volume VI – heterogeneous reactions with liquid substrates, *Atmos. Chem. Phys.*, 13, 8045–8228, doi:10.5194/acp-13-8045-2013, 2013.
- Banham, S. F., Sodeau, J. R., Horn, A. B., McCoustra, M. R. S., and Chesters, M. A.: Adsorption and ionization of HCl on an ice surface, *J. Vac. Sci. Technol. A*, 14, 1620–1626, 1996.
- Broker, W. and Mossman, A. L.: Matheson Gas Data Book, 6th ed., Matheson Gas Products Inc., Lyndhurst, NJ, 1980.
- Carslaw, K. S., Peter, Th., and Clegg, S. L.: Modeling the composition of liquid stratospheric aerosols, *Rev. Geophys.* 35, 125–154, 1997.
- Chiesa, S. and Rossi, M. J.: The metastable HCl • 6H<sub>2</sub>O phase – IR spectroscopy, phase transitions and kinetic/thermodynamic properties in the range 170–205 K, *Atmos. Chem. Phys.*, 13, 11905–11923, doi:10.5194/acp-13-11905-2013, 2013.
- Chu, L. T., Leu, M.-T., and Keyser, L. F.: Uptake of HCl in water ice and nitric acid ice films, *J. Phys. Chem.* 97, 7779–7785, 1993.
- Crowley, J. N., Ammann, M., Cox, R. A., Hynes, R. G., Jenkin, M. E., Mellouki, A., Rossi, M. J., Troe, J., and Wallington, T. J.: Evaluated kinetic and photochemical data for atmospheric chemistry: Volume V – heterogeneous reactions on solid substrates, *Atmos. Chem. Phys.* 10, 9059–9223, doi:10.5194/acp-10-9059-2010, 2010.
- Deitz, V. R. and Turner, N. H.: Introduction of water vapor into vacuum systems and the adsorption by the walls, *J. Vac. Sci. Technol.*, 7, 577–580, 1970.
- Delval, C., Flückiger, B., and Rossi, M. J.: The rate of water vapor evaporation from ice substrates in the presence of HCl and HBr: implications for the lifetime of atmospheric ice particles, *Atmos. Chem. Phys.* 3, 1131–1145, doi:10.5194/acp-3-1131-2003, 2003.
- Delval, C.: Study of the kinetics of Condensation and Evaporation of Water Vapor over Atmospherically relevant Pure and Doped Ice Films: A Multidiagnostic Approach, Thèse EPFL (Ecole Polytechnique Fédérale de Lausanne) no. 3159, 2005.
- Delzeit, L., Rowland, B., and Devlin, J. P.: Infrared spectra of HCl complexed/ionized in amorphous hydrates and at ice surfaces in the 15–90 K range, *J. Phys. Chem.* 97, 10312–10318, 1993.
- Dushman, S. and Lafferty, J. M.: *Scientific Foundations of Vacuum Technique*, 2nd ed., John Wiley & Sons, New York, 1, p. 58, 1962.
- Flückiger, B., Thielmann, A., Gutzwiller, L., and Rossi, M. J.: Real time kinetics and thermochemistry of the uptake of HCl, HBr and HI on water in the temperature range 190 to 210 K, *Ber. Bunsenges. Phys. Chem.* 102, 915–928, 1998.
- Flückiger, B. and Rossi, M. J.: Common precursor mechanism for the heterogeneous reaction of D<sub>2</sub>O, HCl, HBr and HOBr with Water Ice in the range 170–230 K: Mass accommodation coefficients on ice, *J. Phys. Chem. A* 107, 4103–4115, 2003.
- Friedl, R. R., Goble, J. H., and Sander, S. P.: A kinetic study of the homogeneous and heterogeneous components of the HCl + ClONO<sub>2</sub> reaction, *Geophys. Res. Lett.* 13, 1351–1354, 1986.
- Graham, J. D. and Roberts, J. T.: Formation of HCl • 6H<sub>2</sub>O from ice and HCl under ultrahigh vacuum, *Chemometrics and intelligent laboratory systems* 37, 139–148, 1997.
- Gregg, S. J. and Sing, K. S. W.: *Adsorption, Surface Area and Porosity*, second edition, Academic Press, London, 195–207, 1982.
- Haynes, W. M., Bruno, T. J., and Lide, D. R. (eds.): *Handbook of Chemistry and Physics*, 94th Edition (Internet Version 2014), CRC Press/Taylor and Francis, Boca Raton, FL, 2668 pp., 2013.
- Hanson, D. R. and Mauersberger, K.: HCl/H<sub>2</sub>O Solid-Phase Vapor Pressures and HCl Solubility in Ice, *J. Phys. Chem.* 94, 4700–4705, 1990.
- Hanson, D. R. and Ravishankara, R.: Investigation of the reactive and nonreactive processes involving ClONO<sub>2</sub> and HCl on water and nitric acid doped ice, *J. Phys. Chem.* 96, 2682–2691, 1992.
- Henson, B. F., Wilson, K. R., Robinson, J. M., Noble, C. A., Casson, J. L., and Worsnop, D. R.: Experimental isotherms of HCl on H<sub>2</sub>O ice under stratospheric conditions: Connections between bulk and interfacial thermodynamics, *J. Chem. Phys.* 121, 8486–8499, 2004.
- Huthwelker, T., Malmström, M. E., Helleis, F., Moortgat, G. K., and Peter, Th.: Kinetics of HCl Uptake on Ice at 190 and 203 K: Implications for the Microphysics of the Uptake Process, *J. Phys. Chem. A* 108, 6302–6318, 2004.
- Hynes, R. G., Mössinger, J. C., and Cox, R. A.: The interaction of HCl with water-ice at tropospheric temperatures, *Geophys. Res. Lett.* 28, 2827–2830, 2001.
- Koehler, B. G., McNeill, L., Middlebrook, A. M., and Tolbert, M. A.: Fourier transform infrared studies of the interaction of HCl with model polar stratospheric cloud films, *J. Geophys. Res.* D98, 10563–10571, 1993.
- Kuhs, W. F., Sippel, Ch., Falenty, A., and Hansen, Th. C.: Extent and relevance of stacking disorder in “ice I<sub>c</sub>”, *PNAS* 109, 21259–21264, 2012.
- Marti, J. and Mauersberger, K.: A Survey and New Measurements of Ice Vapor Pressure at Temperatures Between 170 and 250 K, *Geophys. Res. Lett.* 20, 363–366, 1993.
- McNeill, V. F., Loerting, T., Geiger, F. M., Trout, B. L., and Molina, M. J.: Hydrogen chloride-induced surface disordering on ice, *Proc. Natl. Acad. Sci. USA*, 103, 9422–9427, 2006.
- McNeill, V. F., Geiger, F. M., Loerting, T., Trout, B. L., Molina, L. T., and Molina, M. J.: Interaction of hydrogen chloride with ice surfaces: The effects of grain size, surface roughness and surface disorder, *J. Phys. Chem. A*, 111, 6274–6284, 2007.
- Molina, L. T., Molina M. J., Stachnik, R. A., and Tom, R. D.: An upper limit to the rate of the HCl + ClONO<sub>2</sub> reaction, *J. Phys. Chem.*, 89, 3779–3781, 1985.
- Molina, M. J.: The Probable Role of Stratospheric ‘Ice’ Clouds: Heterogeneous Chemistry of the Ozone Hole, in: *The Chemistry of the Atmosphere: Its Impact on Global Change*, Blackwell Scientific Publications, London, ch. 3, 27–38, 1994.
- Molina, M. J., Tso, T. L., Molina, L. T., and Wang, F. C. Y.: Antarctic stratospheric chemistry of chlorine nitrate, hydrogen chloride and ice: release of active chlorine, *Science*, 238, 1253–1257, 1987.
- Parent, Ph., Lasne, J., Marcotte, G. and Laffon, C.: HCl adsorption on ice at low temperature: a combined X-ray absorption, photoemission and infrared study, *Phys. Chem. Chem. Phys.* 13, 7142–7148, 2011.

- Peter, Th.: Microphysics and heterogeneous chemistry of Polar Stratospheric Clouds, *Annu. Rev. Phys. Chem.*, 48, 785–822, 1997.
- Pouvesle, N., Kippenberger, M., Schuster, G., and Crowley, J. N.: The interaction of H<sub>2</sub>O<sub>2</sub> with ice surfaces between 203 and 233 K, *Phys. Chem. Chem. Phys.* 12, 15544–15550, 2010.
- Répánszki, R., Kerner, Z., and Nagy, G.: Adsorption of fission products on stainless steel and zirconium, *Adsorption*, 13, 201–207, 2007.
- Ritzhaupt, G. and Devlin, J. P.: Infrared spectra of nitric and hydrochloric acid hydrate thin films, *J. Phys. Chem.*, 95, 90–95, 1991.
- Sadtchenko, V., Giese, C. F., and Gentry, W. R.: Interaction of hydrogen chloride with thin ice films: The effect of ice morphology and evidence for unique surface species on crystalline vapor-deposited ice, *J. Phys. Chem. B* 104, 9421–9429, 2000.
- Seinfeld, J. H. and Pandis, S. N.: *Atmospheric Chemistry and Physics: From air pollution to Climate Change*, 2nd ed., ch.5, John Wiley & Sons, New York, 2006.
- Solomon, S., Garcia, R. R., Rowland, F. S., and Wuebbles, D. J.: On the depletion of Antarctic ozone, *Nature* 321, 755–758, 1986.
- Toon, O. B., Tolbert, M. A., Koehler, B. G., Middlebrook, A. M., and Jordan, J.: Infrared optical constants of H<sub>2</sub>O ice, amorphous nitric acid solutions, and nitric acid hydrates, *J. Geophys. Res.* 99, 631–654, 1994.
- von Hessberg, P., Pouvesle, N., Winkler, A. K., Schuster, G., and Crowley, J. N.: Interaction of formic and acetic acid with ice surfaces between 187 and 117 K. Investigation of single species- and competitive adsorption, *Phys. Chem. Chem. Phys.*, 10, 2345–2355, 2008.
- Wagman, D. D., Evans, W. H., Parker, V. B., Schumm, R. H., Halow, I., Bailey, S. M., Churney, K. L., and Nuttall, R. L.: NBS tables of chemical thermodynamic properties – Selected values for inorganic and C<sub>1</sub> and C<sub>2</sub> organic substances in SI units, *J. Phys. Chem. Ref. Data*, 11, Suppl. 2, 1982.
- Winkler, A. K., Holmes, N. S., and Crowley, J. N.: Interaction of methanol, acetone and formaldehyde with ice surfaces between 198 and 223 K, *Phys. Chem. Chem. Phys.* 4, 5270–5275, 2002.
- Wooldridge, P. J., Zhang, R., and Molina, M. J.: Phase Equilibria of H<sub>2</sub>SO<sub>4</sub>, HNO<sub>3</sub> and HCl hydrates and the composition of polar stratospheric clouds, *J. Geophys. Res.*, 100, 1389–1396, 1995.
- Xueref, I. and Dominé, F.: FTIR spectroscopic studies of the simultaneous condensation of HCl and H<sub>2</sub>O at 190 K – Atmospheric applications, *Atmos. Chem. Phys.*, 3, 1779–1789, doi:10.5194/acp-3-1779-2003, 2003.
- Zondlo, M. A., Hudson, P. K., Prenni, A. J., and Tolbert, M. A.: Chemistry and microphysics of polar stratospheric clouds and cirrus clouds, *Ann. Rev. Phys. Chem.*, 51, 473–499, 2000.